Yesiltepe *et al.*
Cell Communication and Signaling (2024) 22:458
https://doi.org/10.1186/s12964-024-01832-2

Cell Communication and Signaling

RESEARCH

Open Access

Analysis of early effects of human APOE isoforms on Alzheimer's disease and type III hyperlipoproteinemia pathways using knock-in rat models with humanized APP and APOE

Metin Yesiltepe[1], Tao Yin[1], Marc Tambini[1], Hanmei Bao[2], Meixia Pan[2], Cristina d'Abramo[3], Luca Giliberto[3,4], Xianlin Han[2,5] and D'Adamio Luciano[1*]

Abstract

APOE is a major genetic factor in late-onset Alzheimer's disease (LOAD), with APOE4 increasing risk, APOE3 acting as neutral, and APOE2 offering protection. APOE also plays key role in lipid metabolism, affecting both peripheral and central systems, particularly in lipoprotein metabolism in triglyceride and cholesterol regulation. APOE2 is linked to Hyperlipoproteinemia type III (HLP), characterized by mixed hypercholesterolemia and hypertriglyceridemia due to impaired binding to Low-Density Lipoproteins receptors. To explore the impact of human APOE isoforms on LOAD and lipid metabolism, we developed Long-Evans rats with human *APOE2*, *APOE3*, or *APOE4* in place of rat *Apoe*. These rats were crossed with those carrying a humanized *App* allele to express human Aβ, which is more aggregation-prone than rodent Aβ, enabling the study of human APOE-human Aβ interactions. In this study, we focused on 80-day-old adolescent rats to analyze early changes that may be associated with the later development of LOAD. We found that *APOE2*$^{hA\beta}$ rats had the highest levels of APOE in serum and brain, with no significant transcriptional differences among isoforms, suggesting variations in protein translation or stability. Aβ43 levels were significantly higher in male *APOE4*$^{hA\beta}$ rats compared to *APOE2*$^{hA\beta}$ rats. However, no differences in Tau or phosphorylated Tau levels were observed across the APOE isoforms. Neuroinflammation analysis revealed lower levels of IL13, IL4 and IL5 in *APOE2*$^{hA\beta}$ males compared to *APOE4*$^{hA\beta}$ males. Neuronal transmission and plasticity tests using field Input-Output (I/O) and long-term potentiation (LTP) recordings showed increased excitability in all APOE-carrying rats, with LTP deficits in *APOE2*$^{hA\beta}$and *APOE4*$^{hA\beta}$ rats compared to *Apoe*$^{hA\beta}$ and *APOE3*$^{hA\beta}$ rats. Additionally, a lipidomic analysis of 222 lipid molecular species in serum samples showed that *APOE2*$^{hA\beta}$ rats displayed elevated triglycerides and cholesterol, making them a valuable model for studying HLP. These rats also exhibited elevated levels of phosphatidylglycerol, phosphatidylserine, phosphatidylethanolamine, sphingomyelin, and lysophosphatidylcholine. Minimal differences in lipid profiles between *APOE3*$^{hA\beta}$ and *APOE4*$^{hA\beta}$ rats reflect findings from mouse models. Future studies will include comprehensive lipidomic analyses in various CNS regions and at older ages to further validate these models and explore the effects of *APOE* isoforms on lipid metabolism in relation to AD pathology.

*Correspondence:
D'Adamio Luciano
luciano.dadamio@rutgers.edu
Full list of author information is available at the end of the article

Introduction

The *Apolipoprotein E* (*APOE*) gene plays an important role in both lipid metabolism and neurological functions. In humans, there are three forms of *APOE*: *APOE2*, *APOE3*, and *APOE4*. These forms are distinguished by the presence of either arginine or cysteine residues at positions 112 and 158. *APOE4*, the ancestral form of *APOE*, is has arginine residues at positions 112 and 158 [1] and is present in about 12% of the population. *APOE3* is the most common variant in contemporary human populations with a prevalence of 69-82% depending on geolocation [2]. *APOE3* emerged later through an arginine-to-cysteine substitution at position 112 of *APOE4*, dating back approximately 200,000 years based on time-depth analysis and natural selection assumptions [3]. The fact that *APOE3* is more recent compared to *APOE4*, yet significantly more prevalent, implies a positive selection pressure favoring *APOE3*. *APOE2*, the least common variant, originated around 80,000 years ago from an arginine-to-cysteine substitution at position 158 of the *APOE3* gene. *APOE* is predominantly expressed in hepatocytes, macrophages, and astrocytes, a type of glial cell in the brain [4, 5].

APOE is genetically linked to late-onset sporadic Alzheimer's disease (LOAD), with *APOE4* being a significant risk factor, *APOE3* considered the "neutral" allele, and *APOE2* exerting a protective role against LOAD [6, 7]. The prevailing hypothesis linking APOE to LOAD suggests that Aβ production and deposition vary with APOE isoforms. Aβ, the primary component of amyloid plaques that characterize AD pathology, originates from sequential cleavage of the Amyloid-β Precursor Protein (APP) by β- and γ-secretases (known as the amyloidogenic processing pathway). APOE isoforms likely influence Aβ production by modulating lipid metabolism and the lipid composition of cellular membranes, with APOE4 promoting amyloidogenic APP cleavage and Aβ production more than APOE3 [8–10]. Moreover, APOE facilitates Aβ clearance and inhibits its aggregation through the formation of APOE-Aβ complexes, with APOE3-Aβ complexes being approximately 20 times more prevalent than APOE4-Aβ complexes [11, 12]. Additionally, APOE isoforms may impact neurite growth differently [13] and affect neuronal cell survival in an isoform-dependent manner [14].

To investigate the impact of human APOE isoforms on LOAD, we developed Long-Evans rats with the rat *Apoe* gene replaced by human *APOE2*, *APOE3*, or *APOE4* variants. Given that the pathogenic mechanisms linked to *APOE4* may significantly influence LOAD pathogenesis through its effects on Aβ production and metabolism via direct interaction with Aβ, we crossed these human *APOE* replacement rats with rats carrying a humanized *App* allele (App^{h} allele) [13]. Humanization of *App* targeted the Aβ region via humanization of the three amino acid differences between rodent and human Aβ. Therefore, these rat models, designated as $APOE2^{hA\beta}$, $APOE3^{hA\beta}$ and $APOE4^{hA\beta}$, are expected to physiologically express both human *APOE* isoforms and human Aβ.

These amino acids differences in Aβ may be crucial as human Aβ is more prone to aggregation compared to its rodent counterpart. In addition, rodent Aβ may not interact as effectively with human APOE as human Aβ does, which could reduce the ability to accurately study pathogenic and physiological mechanisms based on APOE-Aβ interactions. This setup enables the investigation of mechanisms underlying the interaction between human APOE and human Aβ. These new rat models represent an advancement compared to earlier rodent models carrying human *APOE* variants, as they now allow for a comprehensive exploration of the interplay between human *APOE* and human Aβ that was not possible in these earlier models [14–16].

We selected rats for these LOAD models because they offer distinct advantages for studying neurodegenerative diseases. Rats are preferred for behavioral, memory, and cognitive research due to their physiological similarities to humans and their high learning capacity [17–20]. The larger size of the rat brain facilitates several procedures crucial to dementia research, including in vivo brain imaging techniques like MRI [21] and PET [22–24], which achieve better spatial resolution in rats, allowing for detailed assessment of neurodegeneration. Rats also support more accessible in vivo electrophysiological recordings and cerebrospinal fluid sampling for biomarker detection. Gene expression differences suggest that rats may be advantageous model of neurodegenerative diseases over mice. Alternative spicing of *MAPT,* which codes for Tau, the protein that forms Neuro Fibrillary Tangles and is mutated in Frontotemporal Dementia [25–27], leads to expression of Tau isoforms with three or four microtubule binding domains (3R and 4R, respectively). Adult human and rat brains express both 3R and 4R Tau isoforms [28]: in contrast, adult mouse brains express only 4R tau [29], suggesting that the rat may be a better model organism for dementias with tauopathy.

APOE also plays a crucial role in lipid metabolism, both peripherally and in the central nervous system. Plasma APOE circulates in the bloodstream and is associated with chylomicron, very low-density lipoprotein (VLDL), and high-density lipoprotein (HDL) particles, playing a crucial role in their metabolism. Chylomicrons, which are derived from the intestine, and VLDL particles, which come from the liver, are lipolyzed in the bloodstream by an enzyme called lipoprotein lipase (LPL). APOE on the remnant lipoprotein

particles binds to low-density lipoprotein (LDL) receptors, LDL receptor-related proteins (LRP), and heparan sulfate proteoglycans (HSPG) on the surface of liver cells [30]. These remnant particles are then endocytosed by the liver cells and removed from the bloodstream. Some VLDL remnants are cleared quickly, while others undergo further lipolysis and are gradually converted into intermediate-density lipoprotein (IDL) and eventually into LDL [31]. LDL particles do not contain APOE, and their removal from the bloodstream is facilitated by the binding of another protein, APOB, to the LDL receptor (LDLR) [32]. APOE is also crucial for the production of VLDL particles. Its expression within liver cells promotes the assembly and secretion of VLDL particles. Optimal expression of APOE is essential for the normal metabolism of triglyceride (TG)-rich lipoproteins. However, overexpression or accumulation of APOE stimulates the production of VLDL triglycerides [33], leading to hypertriglyceridemia. Additionally, an excess of APOE on VLDL particles can hinder their lipolysis [34], resulting in elevated plasma triglyceride levels.

The critical role of APOE in lipid metabolism is underscored by evidence showing that *APOE2* homozygosity can lead to Hyperlipoproteinemia type III (HLP), characterized by mixed hypercholesterolemia and hypertriglyceridemia [35–39]. This is attributed to the fact that the cysteine change at position 158 in APOE2, near the LDLR binding region, hinders *APOE2* binding to the LDLR [30, 40]. In addition, *APOE4* is linked to hypercholesterolemia and increased risk of cardiovascular disorders (CVD) [7, 41], although the specific underlying mechanism remains unclear [39, 42].

In this study, we provide an initial characterization of $APOE2^{hA\beta}$, $APOE3^{hA\beta}$ and $APOE4^{hA\beta}$ rats, focusing on early effects (~80-day-old adolescent rats) of these APOE isoforms on APP processing, Tau phosphorylation, neuroinflammation, synaptic plasticity, and plasma lipidomics. Our findings may highlight early changes associated with *APOE* isoforms that could later impact LOAD risk, potentially through alterations in APP processing, Tau metabolism, and lipid pathways.

Materials and methods

Animals

All experiments were done according to policies on the care and use of laboratory animals of the Ethical Guidelines for Treatment of Laboratory Animals of the NIH. Relevant protocols were approved by the Rutgers Institutional Animal Care and Use Committee (Protocol #201702513). All efforts were made to minimize animal suffering and reduce the number of rats used.

Generation of Long-Evans rat models expressing human APOE variants with human APP gene

gRNAs targeting vectors and the donor vector, which is flanked by homologous arms, were constructed and confirmed by sequencing (designed as shown below). The vectors' sequences are available at the indicated links.

gRNA designed:

gRNA1 (matches forward strand of gene): AATCACAACTGGGAAGATGAAGG
gRNA2 (Cas9_D10A) (matches reverse strand of gene): TTCATCTTCCCAGTTGTGATTGG
gRNA3 (Cas9_D10A) (matches forward strand of gene): AATCACAACTGGGAAGATGAAGG

Links the the gRNA and donor vectors on VectorBuilder:

gRNA1: https://www.vectorbuilder.com/vector/VB171212-1056smp.html
gRNA2 (Cas9_D10A): https://www.vectorbuilder.com/vector/VB171212-1329ath.html
gRNA3 (Cas9_D10A): https://www.vectorbuilder.com/vector/VB171212-1058ubb.html
Donor vector for *APOE2* plus SV40 late polyadenylation site flanked by homologous arms: https://www.vectorbuilder.com/vector/VB171225-1186ayg.html
Donor vector for *APOE3* plus SV40 late polyadenylation site flanked by homologous arms: https://www.vectorbuilder.com/vector/VB171225-1189pmt.html
Donor vector for *APOE4* plus SV40 late polyadenylation site flanked by homologous arms: https://www.vectorbuilder.com/vector/VB171225-1191dnt.html

Cas9 mRNA, gRNA generated by in vitro transcription, and oligo donor were co-injected into fertilized eggs to generate knock-in (KI) rats. The PCR primer pairs used to determine correct KI insertion and the integrity of the APOE sequences' insertions were as follows (5' to 3'):

SPF1: CACCCGTGGCAGAGGAATCAAC x SPR1: TTCTAGCGGGTCGGGTCGTCT
SPF2: CCAACCCCCTTCATCTGGATTTC x SPR2: AAAGGTCAGAATTAGGGTGGGAGG'
KI-1-F:TGCTCTATTGTGGAGATGTTTGTGATG x KI-1-R: GTGTGGGGGTGATGGAGAATAAAG ATC
KI-2-F: CCACACCCGACTAACTTTTTTGTATTTTC x KI-2-R: TCAACTCCTTCATGGTCTCGTCCATC
KI-3-F: GCCTCCTAGCTCCTTCTTCGTCTCTG x KI-3-R: CAGGCGTATCTGCTGGGCCTG

KI-4-F: TAAGCGGCTCCTCCGCGATG x KI-4-R: AGCAGAATCGCTTGAACCCAAGAG
KI-5-F: CCTCAGTTTCTCTTTCTGCCCACATA x KI-5-R: TATTATGGATAGGGAAAGACAAGG CC

The primers used for the Southern blot analysis were:

5' arm Probe: F: CCAAGATTATACATCCGGCAA CCG x R: GGCTGGAGGCTTAAATGGAAATAGG
3' arm Probe: F: TGTTGGTCCCATTGCTGACAG GTA x R: AAGCAACAGTGCGTCTGGAAGTCAG

To generate *APOE2*$^{hA\beta}$, *APOE3*$^{hA\beta}$ and *APOE4*$^{hA\beta}$ rats, we doubly crossed humanized *APOE* rats described above with *App*$^{h/h}$ rats that carries *App* genes with the humanized Aβ sequence. The *App*^{h} allele enables the physiological production of human Aβ instead of rodent Aβ from the endogenous rat *App* gene [43–49].

Protein preparation

These procedures were performed as previously described [50]. Briefly, the rats were first put under anesthesia using isoflurane, followed by perfusion through intracardiac catheterization using ice-cold PBS. Brains were extracted and homogenized with a glass-teflon homogenizer in 250 mM Sucrose, 20 mM Tris-base pH 7.4, 1 mM EDTA, 1 mM EGTA plus protease and phosphatase inhibitors (Thermo Scientific). All steps were carried out on the ice. Homogenates were solubilized with 1% NP-40 for 30 min rotating and spun at 20,000 g for 10 min. Supernatants were collected and protein content was quantified using the Bradford method.

Quantitative RT-PCR

Total brain RNA was extracted using the RNeasy RNA Isolation kit (Qiagen) and converted to cDNA using the High-Capacity cDNA Reverse Transcription Kit (Thermo Fisher) with oligo dT priming. For each reaction, 50 ng of cDNA, TaqMan™ Fast Advanced Master Mix (Thermo Fisher 4444556), and the appropriate TaqMan probes (Thermo Fisher) were used. Real-time PCR was conducted on a QuantStudio 6 Flex Real-Time PCR System (Thermo Fisher). Relative RNA quantification was performed using LinRegPCR software (hartfaalcentrum.nl). The rat *Apoe* transcript was detected using probe Rn00593680_m1 targeting exon junction 3–4, while human *APOE* was detected using probe Hs00171168_m1 for the same exon junction. Amplification data were normalized to rat *Gapdh* expression, assessed using probe Rn01775763_g1.

ELISA

For analysis of human APOE, Aβ38, Aβ40, Aβ42, sAPPα and sAPPβSw, the following Meso Scale Discovery kits were used: levels of APOE were measured with R-PLEX Human ApoE Assay (K151AMLR) (serum samples were diluted 1:20,000), Aβ38, Aβ40, and Aβ42 were measured with V-PLEX Plus Aβ Peptide Panel 1 6E10 (K15200G); sAPPα and sAPPβ were measured with sAPPα/sAPPβ kit (K15120E). For analysis of Aβ43, IBL Human Amyloidβ (1–43) (FL) Assay Kit (27710) was used. Cytokines (IFN-γ, IL-1β, IL-4, IL-5, IL-6, IL-10, IL-13, CXCL1, and TNF-α) were measured with V-PLEX Proinflammatory Panel 2 Rat Kit (K15059D). All measurements were performed according to the manufacturer's recommendations. Plates were read on a MESO QuickPlex SQ 120.

Western blots (WB)

WB were performed as follows: proteins were diluted with PBS and LDS Sample Buffer (Invitrogen NP0007) containing 10% β-mercaptoethanol, and 4.5M urea to a concentration of 1 μg/μl. Samples were loaded onto a 4–12% Bis-Tris polyacrylamide gel (Biorad 3450125) and transferred onto nitrocellulose membranes at 25 V for 7 minutes using the Trans-Blot Turbo system (Biorad). Blotting efficiency was confirmed by red Ponceau staining of the membranes.

Membranes were blocked for 45 minutes in 5% milk (Biorad 1706404), followed by extensive washing in PBS/Tween20-0.05%. Primary antibodies (anti-APOE Rabbit mAb, Cell Signaling Technology, 10197SF; anti-APP (Y188) Rabbit mAb, Abcam, Ab32136; anti-GAPDH Rabbit mAb, Sigma, g9545; anti-PSD95, Cell Signaling Technology, 3450) were used at 1:1000 dilution overnight at 4°C. Additionally, we used the following anti-Tau monoclonal antibodies developed by Dr. Peter Davies, at a 1:500 dilution: Total Tau (DA9), Tau-pS^{202} (CP13), Tau-pT^{231} (RZ3), and Tau-pS$^{396\text{-}404}$ (PHF1).

After washing three times for 10 minutes each with PBS/Tween20-0.05%, membranes were incubated with a mixture of HRP-conjugated anti-rabbit secondary antibodies (Southern Biotech, OB405005 and Cell Signaling Technology, 7074) diluted 1:1,000 in 5% milk for 45 minutes at room temperature with shaking. Blots were developed using Clarity Western ECL reagent (Bio-rad 1705061) and visualized on a ChemiDoc MP Imaging System (Bio-Rad). For WB quantifications, signal intensities were analyzed with Image Lab software (Bio-Rad).

Hippocampal electrophysiology experiments

Electrophysiology recordings employed in this study closely follow the experimental procedures outlined in our previously published work [51]. The rats were first

anesthetized using isoflurane (Covetrus, OH) and intracardiac perfusion was performed using ice-cold cutting solution (120 mM choline chloride, 26 mM NaHCO3, 15 mM D-Glucose, 2.6 mM KCl, 1.25 NaH2PO4, 1.3 mM ascorbic acid, 7 mM MgCl2, and 0.5 mM CaCl2). The brains were removed from the skull and rapidly placed in ice-cold cutting solution bubbled with 95% O2 / 5% CO2. Coronal brain slices of 300 µm thickness were then prepared using a Vibratome VT1200S (Leica, Germany). The hippocampal formations were carefully dissected using a microsurgical knife (Electron Microscopy Sciences, CA), and hippocampal slices were incubated for 1 h in artificial cerebrospinal fluid (ACSF, 124 mM NaCl, 26 mM NaHCO3, 10 mM D-Glucose, 3 mM KCl, 1 mM MgSO4, 1.25 mM KH2PO4 and 2 mM CaCl2), bubbling with 95% O2/5% CO2 at 30°C. Later hippocampal slices were transferred to the multielectrode dish (MED-515A, Alpha MED Scientific Inc, Japan) with a 150µm interelectrode distance. The chamber was perfused with oxygenated ACSF at a flow rate of 1.5-2 mL/min, at 32°C. Basal field excitatory postsynaptic potentials (fEPSP) were generated by stimulating Schaffer collaterals at 0.05 Hz and all recordings were done in stratum radiatum layer of CA1 hippocampal region. For input/output curves (I/O) the stimulation strength was increased from -5 to -80 µA in steps of 5 µA. The threshold stimulus was determined as the stimulus strength needed to generate 30–40% of the maximum fEPSP amplitude during I/O curve recordings. The long-term potentiation (LTP) was induced after 15 min of baseline recording with a Θ-burst stimulation. Θ-burst stimulation parameters; Burst = 4 pulses with threshold stimulus at 100 Hz (10 ms pulse-intervals). This burst was repeated 10 times at 5 Hz and named as a train (200 ms burst-intervals). 4 trains of 10-bursts were administered at 10 s intervals (in total 40 bursts were applied). LTP was analyzed in 3 different phases; short term potentiation (STP, 11–20 m), early-LTP (E-LTP, 51–60 m) and late-LTP (L-LTP, 111–120 m). Data were filtered at 1 kHz, digitized at 20 kHz and analyzed with Mobius software (Alpha MED Scientific Inc, Japan).

Blood glucose and lipid profile measurements

Blood glucose levels were measured using the ACCU-CHEK Guide Me system (Roche, mg/dL). For the blood lipid profile, including total cholesterol (TC, range 100-450 mg/dL), HDL (range 25-95 mg/dL), LDL (calculated), and TG (range 45-450 mg/dL), a CURO L7 Lipid Analyzer (CUROfit, CA) cholesterol home test kit was utilized. Briefly, blood was collected via cardiac puncture from 80-day-old rats (with a sample size of 4 per sex per genotype). 35 µL of fresh blood was applied to a lipid profile test strip and measured after 3 minutes. Measurements falling below the specified range were rounded up to the closest integer within the lower end, while those above the range were rounded down to the closest integer within the upper end. LDL levels were calculated using the Friedewald equation: LDL (mg/dL) = TC - HDL - (TG/5).

Lipidomic analysis

Serum for lipidomic analysis was collected from the same rats used for blood glucose and lipid profile measurements. Blood was drawn into serum separator tubes (BD Becton Dickinson vacutainers, SSTTM) and left to incubate at room temperature for 30 minutes. The tubes were then centrifuged at 2000×g for 10 minutes to separate the serum, which was subsequently stored at -80°C.

For lipidomic analysis, the protein content of the thawed serum samples was quantified using a BCA protein assay kit (Pierce, Rockford, IL, USA). A mixture of approximately 20 internal standards was added to serum samples based on the protein content for quantification of individual lipid molecular species as previously described [52]. The extraction of lipids was carried out using a modified Bligh and Dyer extraction method, as previously described [53]. Multi-dimensional mass spectrometry (MDMS)-based shotgun lipidomics (MDMS-SL) was performed using electrospray ionization mass spectrometry (ESI/MS) to measure individual lipid molecular species [54–56]. Instrumentation utilized was a triple-quadruple mass spectrometer (Thermo Scientific TSQ Altis, San Jose, CA, USA) equipped with a NanoMate device (Advion Bioscience Ltd., Ithaca, NY, USA). Xcalibur system software was utilized for this process. Data processing included several steps such as ion peak selection, baseline correction, data transfer, peak intensity comparison, 13C deisotoping, and quantitation. These steps were conducted using a custom-programmed Microsoft Excel macro, as previously described [57]. The concentrations of the total lipid class populations were calculated by summing the individually detected analytes that belonged to the class.

Statistical analysis

Data were analyzed using GraphPad Prism software and expressed as mean ± SEM. Statistical tests used to evaluate significance, and statistical data are shown in tables. Significant differences were accepted at $P < 0.05$.

Results

Generation of Long-Evans rat models expressing either human *APOE2*, *APOE3* or *APOE4* variant genes and the humanized *App* rat gene

The rat *Apoe* gene, with GenBank accession number NM_138828.3 and Ensembl ID ENSRNOG00000018454, is on rat chromosome 1. The gene comprises 4 exons, with the ATG start codon located in exon 2 and the TGA stop codon located in exon 4. Long-Evans rat models expressing human *APOE2*, *APOE3*, and *APOE4* variants were separately generated using CRISPR/Cas-mediated genome engineering. To achieve this, the ATG start codon in exon 2 of the rat *Apoe* gene was replaced with coding sequences for human *APOE2*, *APOE3*, or *APOE4* (Fig. 1a). These human APOE coding sequences were linked to the SV40 late polyadenylation site. By employing the gene manipulation strategy as described above, the expression of human *APOE2*, *APOE3*, and *APOE4* variants, which replaces the expression of the rat *Apoe* gene, is controlled using the regulatory elements of the rat *Apoe* gene. This allows for the accurate and specific regulation of the human *APOE* variants' expression in the Long-Evans rat models. To confirm CRISPR-induced mutations, the resulting pups underwent genotyping by PCR, followed by sequence analysis. PCR was initially performed using primers SPF1 x SPR1 and SPF2 x SPR2 to identify founder rats (F0). Based on this screening, rat 10 was selected as an F0 rat for *APOE2*, rat 26 as an F0 for *APOE3*, and rats 6 and 7 as F0s for *APOE4* (Fig. 1b). Subsequently, the same PCR method was used to identify

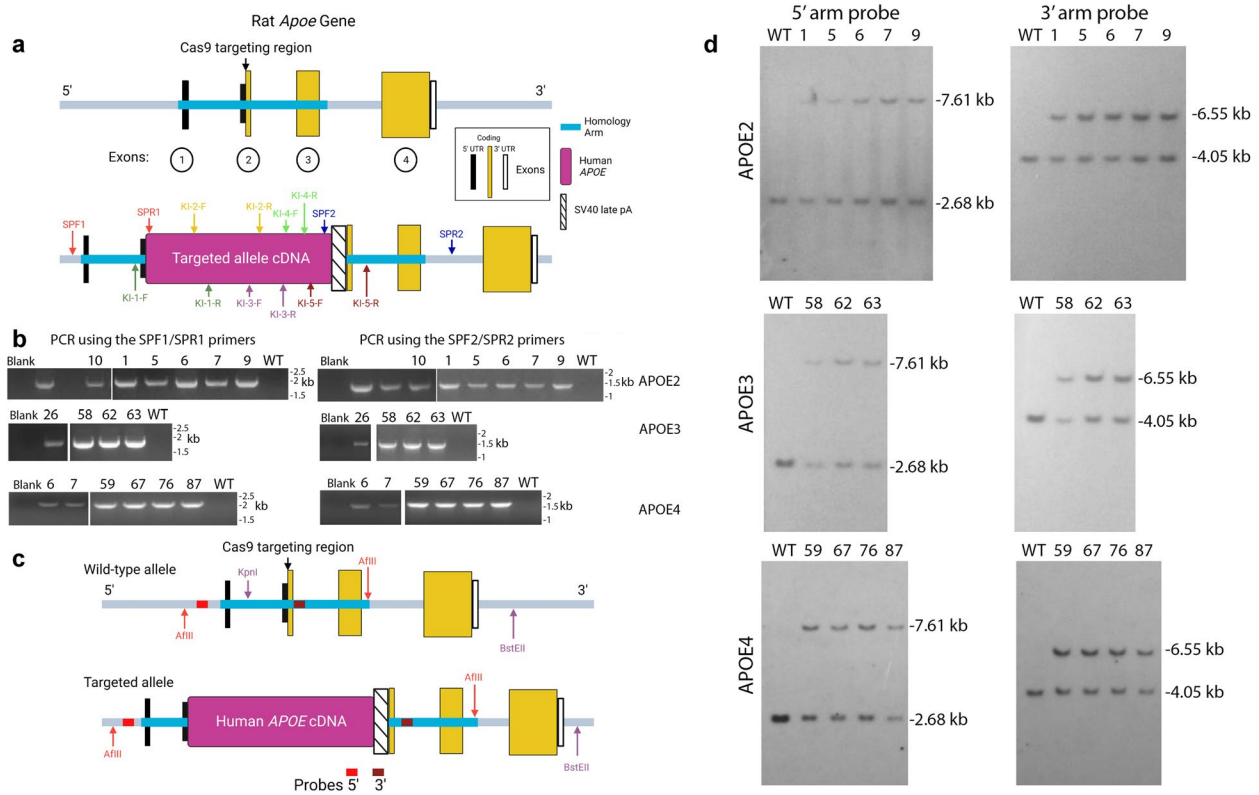

Fig. 1 Generation of humanized *APOE* rats. **a** The schematic representation of the rat *Apoe* allele depicts the four exons with the 5' UTR sequences in black, the coding sequences in orange, and the 3' UTR in white. The regions utilized for the homology arms of the KI construct are indicated in blue. The Cas9 targeting site is also highlighted. Below is a schematic representation of the human *APOE KI* allele, with the sites of the oligonucleotides used for PCR analysis indicated. **b** PCR analysis using primer pairs SPF1/SPR1, which detects correct insertion at the 5' region, and primer pairs SPF2/SPR2, which detects correct insertion at the 3' region. The data show that the rats designed as *APOE2, APOE3,* and *APOE4* F0 and F1 have correct 5' and 3' insertions. **c** The schematic representation of the Southern blotting technique used for genotyping the *APOE2, APOE3,* and *APOE4* rats is presented. For the 5' arm probe Southern blot, genomic DNA was digested with AflII. The expected fragment size for the wild-type rat *Apoe* allele was 2.68 kb, while for the human *APOE KI* allele, it was 7.61 kb. For the 3' arm, genomic DNA was digested with KpnI plus BstEII. The expected fragment size for the wild-type rat *Apoe* allele was 4.05 kb, and for the human *APOE KI* allele, it was 6.55 kb. **d** Southern blot analysis shows that the wild-type sample displayed the expected rat *Apoe* bands of 2.68 kb and 4.05 kb for the 5' arm probe and 3' arm probe, respectively. In contrast, the samples identified as *APOE2, APOE3,* and *APOE4* F1s by the PCR analysis in part b, exhibited both the wild-type bands and the *APOE* KI bands of 7.61 kb and 6.55 kb for the 5' arm probe and 3' arm probe, respectively. No other bands that would indicate off-target, random integration are detected

and designate certain offspring of these F0 rats as *APOE2* F1s (rats 1, 5, 6, 7, and 9), *APOE3* F1s (rats 58, 62, and 63), and *APOE4* F1s (rats 59, 67, 76, and 87) based on their respective parentage (Fig. 1b). The selection of F0 and F1 rats was further validated by PCR using 5 primer pairs (KI-1-F x KI-1-R, KI-2-F x KI-2-R, KI-3-F x KI-3-R, KI-4-F x KI-4-R, and KI-5-F x KI-5-R) followed by sequencing to confirm the genotyping results. The accurate gene targeting in F1 animals was verified through Southern blot analysis of the tail DNA samples. The Southern blot analysis strategy is depicted in Fig. 1c. The results demonstrated that all F1 rats analyzed expressed both the rat *Apoe* allele and the human *APOE* knock-in (KI) allele in a 1:1 ratio (Fig. 1d). F1 rats were crossed to Long Evans for 5 generations. The probability that F5 rats carry unidentified off-target insertions/mutations (except those that may be on Chr. 1) is ~1.5625%.

APOE isoforms have been associated with the risk of LOAD, with *APOE4* increasing the risk and *APOE2* reducing it. Considering the important role of *APP* in LOAD pathogenesis and the interplay between APP, its metabolic product Aβ, and APOE isoforms, we crossed *APOE2*, *APOE3*, and *APOE4* rats with animals carrying a rat *App* allele humanized specifically in the Aβ region ($App^{h/h}$ rats). The resulting progeny, double heterozygous for *APOE* and App^{h} alleles, were further bred to generate rats homozygous for humanized *APOE* and App^{h}, thereby exclusively producing human Aβ species in a physiological manner. These models were designated as $APOE2^{hA\beta}$, $APOE3^{hA\beta}$ and $APOE4^{hA\beta}$. *APP* is expressed in virtually all types of cells, suggesting broader functions beyond the central nervous system (CNS). Studying these double humanized rats could offer significant advantages, particularly in exploring how human APOE's systemic functions related to lipid metabolism are influenced by its interactions with human Aβ. Utilizing $Apoe^{hA\beta}$, $APOE2^{hA\beta}$, $APOE3^{hA\beta}$ and $APOE4^{hA\beta}$ rats for this lipid metabolism study may yield valuable insights into their potential interactions without apparent drawbacks.

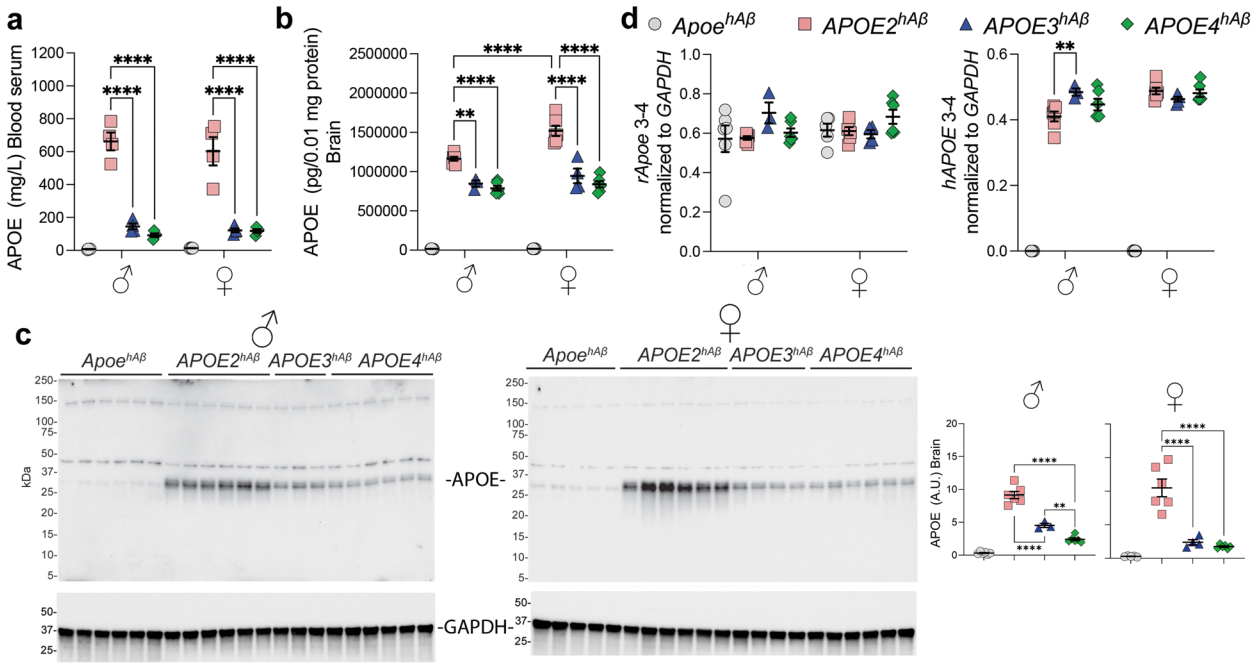

Fig. 2 Levels of human APOE in 80 days old $Apoe^{hA\beta}$, $APOE2^{hA\beta}$, $APOE3^{hA\beta}$ and $APOE4^{hA\beta}$ rats. **a** ELISA measurements of human APOE in blood serum (n=4 per sex per genotype) showed significantly higher levels in $APOE2^{hA\beta}$ compared to $APOE3^{hA\beta}$ and $APOE4^{hA\beta}$ in both males and females. **b** ELISA analysis of human APOE in brain homogenates ($Apoe^{hA\beta}$, females n=6, males n=5; $APOE2^{hA\beta}$, females n=6, males n=6; $APOE3^{hA\beta}$, females n=4, males n=3; $APOE4^{hA\beta}$, females n=6, males n=6) revealed higher levels in $APOE2^{hA\beta}$ compared to $APOE3^{hA\beta}$ and $APOE4^{hA\beta}$ in both sexes. Moreover, brain APOE levels were higher in male $APOE2^{hA\beta}$ rats compared to females. Rat Apoe ($Apoe^{hA\beta}$ rats) is not detected by the ELISA demonstrating specificity. Therefore, $Apoe^{hA\beta}$ rats were excluded from the statistical analysis. **c** WB analysis of human APOE in the same brains analyzed by ELISA in panel b confirms higher levels of APOE in $APOE2^{hA\beta}$ brains compared to $APOE3^{hA\beta}$ and $APOE4^{hA\beta}$ in both sexes. **d** Quantitative RT-PCR analysis of rat and human *APOE* mRNA expression in the same brains analyzed by ELISA and WB in panels b and c confirms that $Apoe^{hA\beta}$ rats express only rat *Apoe* mRNA, while $APOE2^{hA\beta}$, $APOE3^{hA\beta}$ and $APOE4^{hA\beta}$ express exclusively human *APOE* mRNA. Human *APOE* mRNA expression levels were comparable among $APOE2^{hA\beta}$, $APOE3^{hA\beta}$ and $APOE4^{hA\beta}$ rats, except for a reduction observed in $APOE2^{hA\beta}$ males compared to $APOE2^{hA\beta}$, $APOE3^{hA\beta}$ males. The WB analysis for GAPDH confirms equal loading of the samples. Data are presented as mean ± SEM and were analyzed by two-way ANOVA followed by post hoc Tukey's multiple comparisons test when significant differences were detected. Statistical significance is denoted as ** p<0.01, *** p<0.001, **** p<0.0001

Table 1 Statistical analysis results of Fig. 2

			APOE- Serum	APOE- Brain	*rApoe* 3-4	*hAPOE* 3-4
Two-way ANOVA summary	Sex-genotype interaction	$F_{(3,24)}$=	0.5074	7.394	1.886	6.310
		p	0.6809	0.0006	0.1506	0.0016
	Sex factor	$F_{(1,24)}$=	0.2308	15.99	0.2219	7.134
		p	0.6353	0.0003	0.6406	0.0115
	Genotype factor	$F_{(3,24)}$=	113.5	344.4	1.282	781.7
		p	<0.0001	<0.0001	0.2963	<0.0001
Post hoc Tukey's Analysis: *p*-Values for Multiple Comparisons						
♂:*Apoe*$^{hA\beta}$vs.♂:*APOE2*$^{hA\beta}$			-	-	-	-
♂:*Apoe*$^{hA\beta}$ vs.♂:*APOE3*$^{hA\beta}$			-	-	-	-
♂:*Apoe*$^{hA\beta}$ vs. ♂:*APOE4*$^{hA\beta}$			-	-	-	-
♂:*Apoe*$^{hA\beta}$ vs. ♀:*Apoe*$^{hA\beta}$			-	-	-	-
♂:*Apoe*$^{hA\beta}$ vs. ♀:*APOE2*$^{hA\beta}$			-	-	-	-
♂:*Apoe*$^{hA\beta}$ vs. ♀:*APOE3*$^{hA\beta}$			-	-	-	-
♂:*Apoe*$^{hA\beta}$ vs. ♀:*APOE4*$^{hA\beta}$			-	-	-	-
♂:*APOE2*$^{hA\beta}$vs. ♂:*APOE3*$^{hA\beta}$			<0.0001	0.0019	0.4291	0.0094
♂:*APOE2*$^{hA\beta}$ vs.♂:*APOE4*$^{hA\beta}$			<0.0001	<0.0001	0.9993	0.3042
♂:*APOE2*$^{hA\beta}$ vs. ♀:*Apoe*$^{hA\beta}$			-	-	-	-
♂:*APOE2*$^{hA\beta}$vs.♀:*APOE2*$^{hA\beta}$			0.9421	<0.0001	0.9963	0.0004
♂:*APOE2*$^{hA\beta}$ vs.♀:*APOE3*$^{hA\beta}$			<0.0001	0.0338	>0.9999	0.0766
♂:*APOE2*$^{hA\beta}$ vs.♀:*APOE4*$^{hA\beta}$			<0.0001	<0.0001	0.3862	0.0015
♂:*APOE3*$^{hA\beta}$ vs.♂:*APOE4*$^{hA\beta}$			0.9672	0.9875	0.7056	0.5075
♂:*APOE3*$^{hA\beta}$ vs. ♀:*Apoe*$^{hA\beta}$			-	-	-	-
♂:*APOE3*$^{hA\beta}$ vs.♀:*APOE2*$^{hA\beta}$			<0.0001	<0.0001	0.7840	>0.9999
♂:*APOE3*$^{hA\beta}$ vs.♀:*APOE3*$^{hA\beta}$			0.9998	0.8996	0.7085	0.9660
♂:*APOE3*$^{hA\beta}$ vs.♀:*APOE4*$^{hA\beta}$			0.9994	>0.9999	>0.9999	>0.9999
♂:*APOE4*$^{hA\beta}$ vs. ♀:*Apoe*$^{hA\beta}$			-	-	-	-
♂:*APOE4*$^{hA\beta}$ vs.♀:*APOE2*$^{hA\beta}$			<0.0001	<0.0001	>0.9999	0.1716
♂:*APOE4*$^{hA\beta}$ vs.♀:*APOE3*$^{hA\beta}$			0.9990	0.2465	>0.9999	0.9783
♂:*APOE4*$^{hA\beta}$ vs.♀:*APOE4*$^{hA\beta}$			0.9996	0.9856	0.7209	0.3637
♀:*Apoe*$^{hA\beta}$ vs. ♀:*APOE2*$^{hA\beta}$			-	-	-	-
♀:*Apoe*$^{hA\beta}$ vs. ♀:*APOE3*$^{hA\beta}$			-	-	-	-
♀:*Apoe*$^{hA\beta}$ vs. ♀:*APOE4*$^{hA\beta}$			-	-	-	-
♀:*APOE2*$^{hA\beta}$ vs.♀:*APOE3*$^{hA\beta}$			<0.0001	<0.0001	>0.9999	0.8396
♀:*APOE2*$^{hA\beta}$ vs.♀:*APOE4*$^{hA\beta}$			<0.0001	<0.0001	0.8134	0.9998
♀:*APOE3*$^{hA\beta}$ vs.♀:*APOE4*$^{hA\beta}$			>0.9999	0.7058	0.7402	0.9649
			APOE Brain-WB			
			♂	♀		
One-way ANOVA summary			$F_{(3, 17)}$ = 130.9, p<0.0001	$F_{(3, 17)}$ = 38.17, p<0.0001		
Apoe$^{hA\beta}$ vs. *APOE2*$^{hA\beta}$			<0.0001	<0.0001		
Apoe$^{hA\beta}$ vs. *APOE3*$^{hA\beta}$			<0.0001	0.3230		
Apoe$^{hA\beta}$ vs. *APOE4*$^{hA\beta}$			0.0018	0.5400		
APOE2$^{hA\beta}$ vs. *APOE3*$^{hA\beta}$			<0.0001	<0.0001		
APOE2$^{hA\beta}$ vs. *APOE4*$^{hA\beta}$			<0.0001	<0.0001		

In the following experiments, we examined adolescent (~80-day-old) *APOE2*$^{hA\beta}$, *APOE3*$^{hA\beta}$ and *APOE4*$^{hA\beta}$ rats to assess the early effects of APOE isoforms on key pathways related to LOAD. This included evaluating APP processing, Tau phosphorylation, neuroinflammation, synaptic plasticity, and plasma lipidomics. Our objective is to identify early alterations associated with APOE isoforms that might influence the risk of developing LOAD later in life.

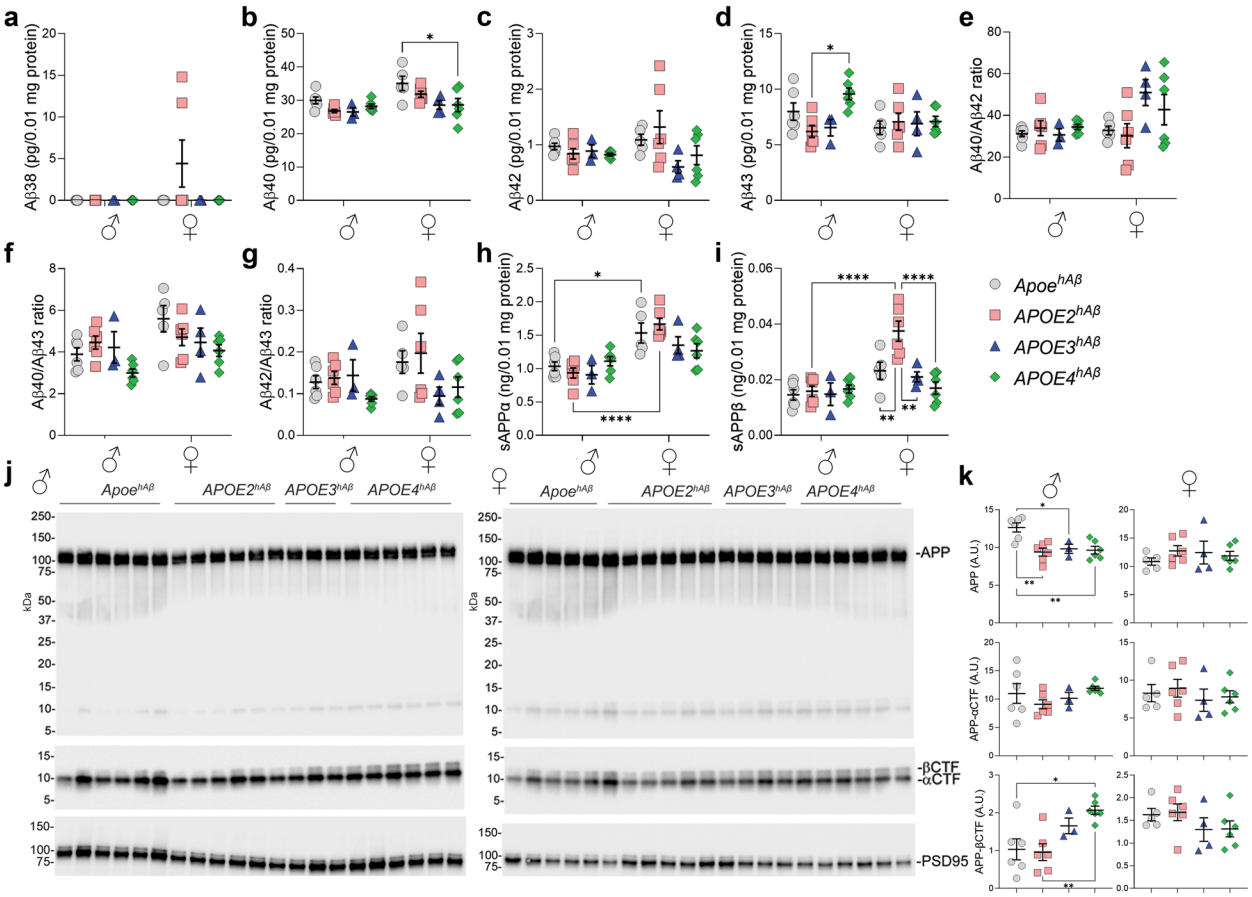

Fig. 3 Analysis of APP metabolites in brains of *Apoe*^{hAβ}, *APOE2*^{hAβ}, *APOE3*^{hAβ} and *APOE4*^{hAβ} rats. **a**-**i** ELISA measurements for Aβ38 (**a**), Aβ40 (**b**), Aβ42 (**c**), Aβ43 (**d**), Aβ40/Aβ42 ratio (**e**), Aβ40/Aβ43 ratio (**f**), Aβ42/Aβ43 ratio (**g**), sAPPα (**h**), and sAPPβ (**i**) were conducted on the same brain homogenates used in Fig. 2b. **j** WB analysis of APP, βCTF, and αCTF in brain lysates used in the WBs shown Fig. 2c. PSD95 WB was used as a loading control. **k** Quantification of the APP, βCTF, and αCTF signals detected in panel j. Longer exposures of βCTF and αCTF signals, which were used to quantify βCTF and αCTF, are shown below the main WBs. Data are represented as mean ± SEM and were analyzed by two-way ANOVA followed by post-hoc Tukey's multiple comparisons tests when ANOVA showed significant differences. Statistical significance is denoted as * $p<0.05$, ** $p<0.01$, *** $p<0.001$, **** $p<0.0001$

Serum and brain APOE levels are highest in *APOE2*^{hAβ} rats

To characterize these models, we first measured human APOE levels in blood serum and brain. Since *Apoe*^{hAβ} rats have rat *Apoe*, we excluded them from this analysis and used them as negative control. Serum APOE levels were highest in *APOE2*^{hAβ} rats in both males and females compared to *APOE3*^{hAβ} and *APOE4*^{hAβ} rats (Fig. 2a; Statistical analysis is in Table 1). Remarkably, this pattern of APOE isoform levels mirrors that found in human serum [58]. Brain APOE levels measured by ELISA were also the highest in *APOE2*^{hAβ} rats compared to *APOE3*^{hAβ} and *APOE4*^{hAβ} rats in both sexes (Fig. 2b; Statistical analysis is in Table 1). Additionally, in the brains of *APOE2*^{hAβ} females, APOE level was higher than male *APOE2*^{hAβ} rats. The ELISA results were confirmed by WB analysis of brain APOE levels (Fig. 2c; Statistical analysis is in Table 1).

To investigate whether the increase in APOE2 protein levels is due to enhanced transcription, we measured mRNA levels of human *APOE2*, *APOE3*, and *APOE4* in *APOE2*^{hAβ}, *APOE3*^{hAβ} and *APOE4*^{hAβ} rats. Overall, these mRNA levels were comparable, with the notable exception of a decrease in *APOE2* mRNA levels in male *APOE2*^{hAβ} compared to male *APOE3*^{hAβ} rats (Fig. 2d), despite APOE2 protein levels being significantly higher than APOE3 levels in male rats (Fig. 2a and b). Therefore, differences in protein expression are likely attributable to translational and/or protein stability variances.

Sex- and APOE isoform-dependent variations in brain APP metabolites

APP is a substrate of several proteases. α-Secretase cleaves APP to produce a soluble ectodomain (sAPPα) and a membrane-bound C-terminal fragment (αCTF).

Table 2 Statistical analysis results of Fig. 3

			Aβ38	Aβ40	Aβ42	Aβ43	Aβ40/Aβ42	Aβ40/Aβ43	Aβ42/Aβ43	sAPPα	sAPPβ
Two-way ANOVA summary	Sex-genotype interaction	$F_{(3,34)}$=	1.978	1.677	1.901	2.735	2.124	1.394	1.241	3.222	7.099
		p	0.1358	0.1902	0.1480	0.0587	0.1154	0.2614	0.3099	0.0347	0.0008
	Sex factor	$F_{(1,34)}$=	1.717	10.53	0.4490	1.840	3.984	7.185	1.209	39.75	25.04
		p	0.1989	0.0026	0.5073	0.1838	0.0540	0.0113	0.2793	<0.0001	<0.0001
	Genotype factor	$F_{(3,34)}$=	1.978	5.083	2.009	2.781	1.791	3.686	2.695	1.152	6.863
		p	0.1358	0.0051	0.1311	0.0558	0.1674	0.0212	0.0613	0.3424	0.0010
Post hoc Tukey's Analysis: *p*-Values for Multiple Comparisons											
♂:$Apoe^{hAβ}$vs.♂:$APOE2^{hAβ}$			>0.9999	0.6177	0.9977	0.5181	0.9998	0.9682	>0.9999	0.9945	>0.9999
♂:$Apoe^{hAβ}$ vs.♂:$APOE3^{hAβ}$			>0.9999	0.7380	>0.9999	0.8921	>0.9999	0.9996	>0.9999	0.9926	>0.9999
♂:$Apoe^{hAβ}$ vs. ♂:$APOE4^{hAβ}$			>0.9999	0.9723	0.9957	0.6518	0.9993	0.7343	0.9438	0.9988	0.9981
♂:$Apoe^{hAβ}$ vs. ♀:$Apoe^{hAβ}$			>0.9999	0.1357	0.9992	0.7869	>0.9999	0.0976	0.8989	0.0195	0.2397
♂:$Apoe^{hAβ}$ vs. ♀:$APOE2^{hAβ}$			0.1075	0.9619	0.6950	0.9694	>0.9999	0.8144	0.5341	0.0007	<0.0001
♂:$Apoe^{hAβ}$ vs. ♀:$APOE3^{hAβ}$			>0.9999	0.9958	0.7394	0.9585	0.0970	0.9822	0.9895	0.4062	0.6674
♂:$Apoe^{hAβ}$ vs. ♀:$APOE4^{hAβ}$			>0.9999	0.9924	0.9931	0.9747	0.5485	>0.9999	>0.9999	0.6449	0.9954
♂:$APOE2^{hAβ}$vs. ♂:$APOE3^{hAβ}$			>0.9999	>0.9999	>0.9999	>0.9999	0.9998	>0.9999	>0.9999	>0.9999	>0.9999
♂:$APOE2^{hAβ}$ vs.♂:$APOE4^{hAβ}$			>0.9999	0.9909	>0.9999	0.0146	>0.9999	0.1766	0.8437	0.8770	>0.9999
♂:$APOE2^{hAβ}$ vs. ♀:$Apoe^{hAβ}$			>0.9999	0.0017	0.9347	>0.9999	>0.9999	0.5225	0.9686	0.0028	0.4316
♂:$APOE2^{hAβ}$vs.♀:$APOE2^{hAβ}$			0.1075	0.1123	0.3023	0.9779	0.9984	0.9998	0.7107	<0.0001	<0.0001
♂:$APOE2^{hAβ}$ vs.♀:$APOE3^{hAβ}$			>0.9999	0.9841	0.9665	0.9968	0.2167	>0.9999	0.9553	0.1230	0.8579
♂:$APOE2^{hAβ}$ vs.♀:$APOE4^{hAβ}$			>0.9999	0.9686	>0.9999	0.9730	0.8177	0.9966	0.9983	0.2216	>0.9999
♂:$APOE3^{hAβ}$ vs.♂:$APOE4^{hAβ}$			>0.9999	0.9917	>0.9999	0.1465	0.9995	0.6163	0.8961	0.9041	0.9998
♂:$APOE3^{hAβ}$ vs. ♀:$Apoe^{hAβ}$			>0.9999	0.0101	0.9926	>0.9999	>0.9999	0.5236	0.9960	0.0133	0.5007
♂:$APOE3^{hAβ}$ vs.♀:$APOE2^{hAβ}$			0.2946	0.2396	0.6729	0.9997	>0.9999	0.9959	0.9196	0.0010	<0.0001
♂:$APOE3^{hAβ}$ vs.♀:$APOE3^{hAβ}$			>0.9999	0.9853	0.9639	>0.9999	0.2108	>0.9999	0.9640	0.2111	0.8479
♂:$APOE3^{hAβ}$ vs.♀:$APOE4^{hAβ}$			>0.9999	0.9761	>0.9999	0.9996	0.7238	>0.9999	0.9979	0.3590	0.9994
♂:$APOE4^{hAβ}$ vs. ♀:$Apoe^{hAβ}$			>0.9999	0.0146	0.9154	0.0528	>0.9999	0.0019	0.2896	0.0750	0.5789
♂:$APOE4^{hAβ}$ vs.♀:$APOE2^{hAβ}$			0.1075	0.4667	0.2701	0.1370	0.9963	0.0674	0.0706	0.0039	<0.0001
♂:$APOE4^{hAβ}$ vs.♀:$APOE3^{hAβ}$			>0.9999	>0.9999	0.9759	0.1760	0.2497	0.2888	>0.9999	0.7333	0.9366
♂:$APOE4^{hAβ}$ vs.♀:$APOE4^{hAβ}$			>0.9999	>0.9999	>0.9999	0.1470	0.8594	0.5315	0.9923	0.9321	>0.9999
♀:$Apoe^{hAβ}$ vs. ♀:$APOE2^{hAβ}$			0.1420	0.6443	0.9606	0.9991	0.9999	0.7897	0.9991	0.9766	0.0059
♀:$Apoe^{hAβ}$ vs. ♀:$APOE3^{hAβ}$			>0.9999	0.0537	0.4674	>0.9999	0.1912	0.6480	0.5198	0.9289	0.9990
♀:$Apoe^{hAβ}$ vs. ♀:$APOE4^{hAβ}$			>0.9999	0.0238	0.8958	0.9987	0.7575	0.1829	0.7415	0.5441	0.6364
♀:$APOE2^{hAβ}$ vs.♀:$APOE3^{hAβ}$			0.1979	0.7099	0.0637	>0.9999	0.0699	>0.9999	0.2010	0.4100	0.0023
♀:$APOE2^{hAβ}$ vs.♀:$APOE4^{hAβ}$			0.1075	0.5935	0.2437	>0.9999	0.4447	0.9396	0.3315	0.0785	<0.0001
♀:$APOE3^{hAβ}$ vs.♀:$APOE4^{hAβ}$			>0.9999	>0.9999	0.9824	>0.9999	0.9210	0.9982	0.9994	0.9991	0.9568

Table 2 (continued)

	Aβ38	Aβ40	Aβ42	Aβ43	Aβ40/Aβ42	Aβ40/Aβ43	Aβ42/Aβ43	sAPPα	sAPPβ
	APP-WB				**APP-αCTF-WB**		**APP-βCTF-WB**		
	♂		♀		♂	♀	♂	♀	
One-way ANOVA summary	$F_{(3, 17)} = 8.105$, p=0.0014		$F_{(3, 17)} = 0.6086$, p=0.6185		$F_{(3, 17)} = 1.214$, p=0.3349	$F_{(3, 17)} = 0.3604$, p=0.7824	$F_{(3, 17)} = 6.218$, p=0.0048	$F_{(3, 17)} = 1.158$, p=0.3546	
Apoe$^{hA\beta}$ vs. *APOE2*$^{hA\beta}$	0.0022		0.5844		0.6078	0.9747	0.9940	0.9974	
Apoe$^{hA\beta}$ vs. *APOE3*$^{hA\beta}$	0.0310		0.7666		0.9694	0.9466	0.3438	0.6682	
Apoe$^{hA\beta}$ vs. *APOE4*$^{hA\beta}$	0.0045		0.9032		0.9305	0.9887	0.0128	0.6298	
APOE2$^{hA\beta}$ vs. *APOE3*$^{hA\beta}$	0.9636		0.9973		0.9396	0.7743	0.2532	0.5341	
APOE2$^{hA\beta}$ vs. *APOE4*$^{hA\beta}$	0.9855		0.9196		0.2870	0.8673	0.0075	0.4762	

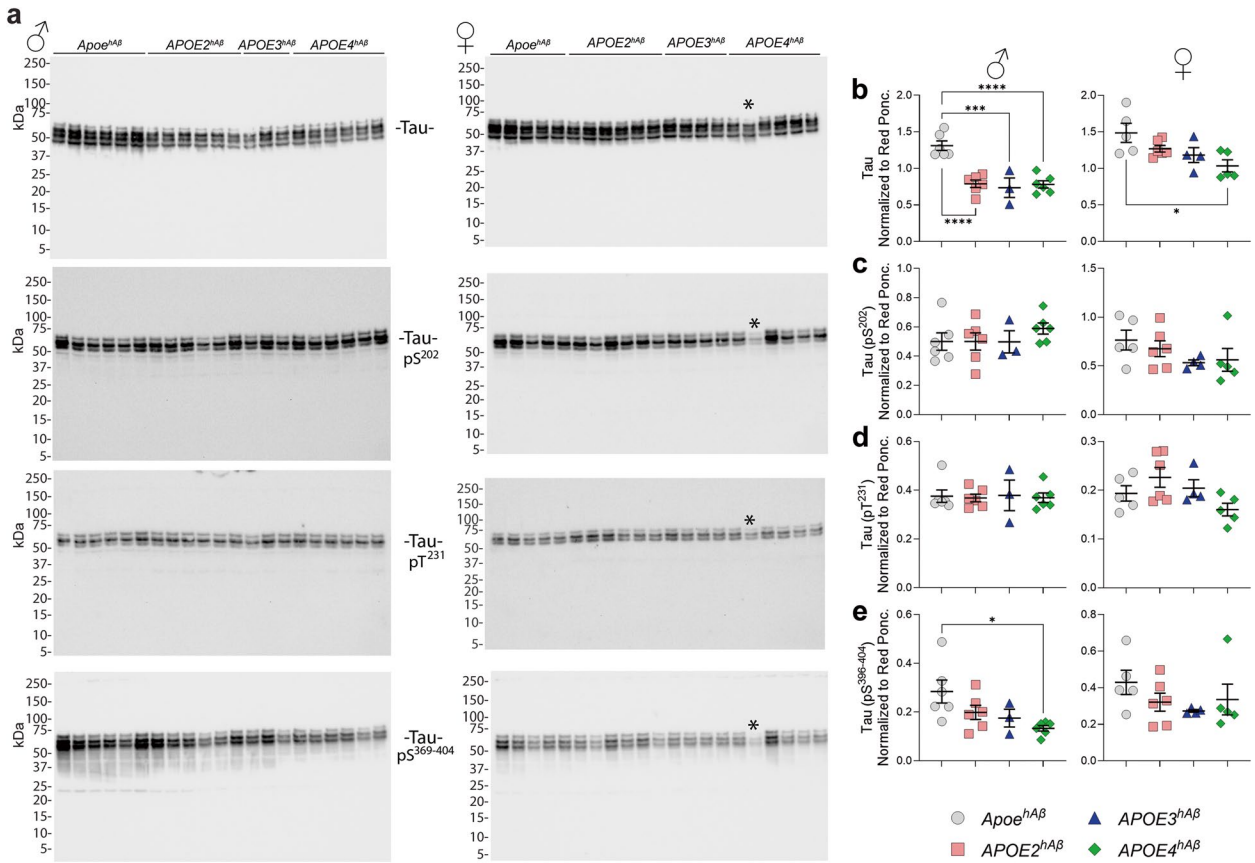

Fig. 4 Analysis of Tau and phosphorylated Tau in brains of *Apoe*^{hAβ}, *APOE2*^{hAβ}, *APOE3*^{hAβ} and *APOE4*^{hAβ} rats. **a** WB analysis of Tau, Tau-pS^{202}, Tau-pT^{231}, Tau pS$^{396-404}$ in brain lysates were conducted on the same brain homogenates used in Fig. 2b (*n*=3-6 per sex per genotype). The star indicates the degraded sample, which was excluded from the analysis. **b**-**e** Quantification of the Tau (**b**), Tau-pS^{202}(**c**), Tau-pT^{231}(**d**), Tau pS$^{396-404}$(**e**) signals detected in panel **a**. Data are represented as mean ± SEM and were analyzed by one-way ANOVA followed by multiple comparisons tests. Statistical significance is denoted as * p<0.05, ** p<0.01, *** p<0.001, **** p<0.0001

Alternatively, β-secretase cleaves APP to generate the soluble sAPPβ ectodomain and the membrane-tethered βCTF stub. Subsequent cleavage of βCTF by γ-secretase leads to the production of Aβ peptides and the short intracellular domain of APP [59]. APOE modulates APP metabolism in an isoform-dependent manner through distinct mechanisms: 1) influencing APP processing via effects on lipid metabolism [8–10], and 2) modulating Aβ clearance and aggregation via the formation of APOE-Aβ complexes [11, 12]. Consequently, we investigated APP metabolites in the CNS of *Apoe*^{hAβ}, *APOE2*^{hAβ}, *APOE3*^{hAβ} and *APOE4*^{hAβ} rats. ELISA experiments showed no significant differences in Aβ38 levels among humanized *APOE* variants (Fig. 3a; Statistical analysis is in Table 2). In female rats, Aβ40 levels were higher in *Apoe*^{hAβ} compared to *APOE4*^{hAβ} rats (Fig. 3b ; Statistical analysis is in Table 2). There was no significant difference in Aβ42 levels and the ratio of Aβ40/Aβ42 across the humanized *APOE* variants (Fig. 3c, e). However, the levels of Aβ43, a determining factor in the onset of pathological amyloid deposition [50], were higher in *APOE4*^{hAβ} males compared to *APOE2*^{hAβ} males, but there was no difference in the Aβ40/Aβ43 or Aβ42/Aβ43 ratios (Fig. 3d, f, g; Statistical analysis is in Table 2). The levels of sAPPα showed sex-specific variations. *Apoe*^{hAβ} and *APOE2*^{hAβ} female rats exhibited higher sAPPα levels compared to males of the same genotype (Fig. 3h; Statistical analysis is in Table 2). Finally, sAPPβ levels were higher in *APOE2*^{hAβ} females compared to all other female groups and *APOE2*^{hAβ} male rats (Fig. 3i; Statistical analysis is in Table 2).

Levels of APP, αCTF and βCTF were quantified by WB, as shown in Fig. 3j. APP levels were higher in *Apoe*^{hAβ} males compared to *APOE2*^{hAβ}, *APOE3*^{hAβ} and *APOE4*^{hAβ} males but no significant differences were observed among females across the APOE variants (Fig. 3k; Statistical analysis is in Table 2). Additionally, there were no differences in αCTF levels in either males or females. However, βCTF levels were higher in

Table 3 Statistical analysis results of Fig. 4

	Tau	
	♂	♀
One-way ANOVA summary	$F_{(3, 17)} = 18.23$, $p<0.0001$	$F_{(3, 16)} = 4.274$, $p= 0.0214$
$Apoe^{hA\beta}$ vs. $APOE2^{hA\beta}$	<0.0001	0.3274
$Apoe^{hA\beta}$ vs. $APOE3^{hA\beta}$	0.0002	0.1581
$Apoe^{hA\beta}$ vs. $APOE4^{hA\beta}$	<0.0001	0.0139
$APOE2^{hA\beta}$ vs. $APOE3^{hA\beta}$	0.9570	0.9091
$APOE2^{hA\beta}$ vs. $APOE4^{hA\beta}$	0.9996	0.2654
	Tau (pS^{202})	
	♂	♀
One-way ANOVA summary	$F_{(3, 17)} = 0.6716$, $p=0.5811$	$F_{(3, 16)} = 1.258$, $p= 0.3221$
$Apoe^{hA\beta}$ vs. $APOE2^{hA\beta}$	>0.9999	0.8933
$Apoe^{hA\beta}$ vs. $APOE3^{hA\beta}$	>0.9999	0.3693
$Apoe^{hA\beta}$ vs. $APOE4^{hA\beta}$	0.6463	0.4367
$APOE2^{hA\beta}$ vs. $APOE3^{hA\beta}$	>0.9999	0.7086
$APOE2^{hA\beta}$ vs. $APOE4^{hA\beta}$	0.6468	0.8021
	Tau (pT^{231})	
	♂	♀
One-way ANOVA summary	$F_{(3, 17)} = 0.03224$, $p=0.9919$	$F_{(3, 16)} = 2.671$, $p= 0.0826$
$Apoe^{hA\beta}$ vs. $APOE2^{hA\beta}$	0.9966	0.5253
$Apoe^{hA\beta}$ vs. $APOE3^{hA\beta}$	0.9999	0.9765
$Apoe^{hA\beta}$ vs. $APOE4^{hA\beta}$	0.9974	0.5448
$APOE2^{hA\beta}$ vs. $APOE3^{hA\beta}$	0.9947	0.8163
$APOE2^{hA\beta}$ vs. $APOE4^{hA\beta}$	>0.9999	0.0563
	Tau ($pS^{396-404}$)	
	♂	♀
One-way ANOVA summary	$F_{(3, 17)}$ 3.906, $p=0.0273$	$F_{(3, 16)} = 1.061$, $p= 0.3933$
$Apoe^{hA\beta}$ vs. $APOE2^{hA\beta}$	0.2649	0.5751
$Apoe^{hA\beta}$ vs. $APOE3^{hA\beta}$	0.2334	0.3571
$Apoe^{hA\beta}$ vs. $APOE4^{hA\beta}$	0.0178	0.7065
$APOE2^{hA\beta}$ vs. $APOE3^{hA\beta}$	0.9724	0.9472
$APOE2^{hA\beta}$ vs. $APOE4^{hA\beta}$	0.4837	0.9980

$APOE4^{hA\beta}$ males compared to $Apoe^{hA\beta}$ and $APOE2^{hA\beta}$ males, with no significant differences observed in females (Fig. 3k; Statistical analysis is in Table 2). PSD95 blots are shown to confirm that these differences were not due to loading variations.

Overall, these findings demonstrated distinct regulation of APP metabolites in relation to *APOE* variants, with notable sex differences.

Similar Tau expression and phosphorylation across APOE isoforms

The microtubule-associated protein Tau maintains axonal microtubule stability in the brain and is involved in regulating axonal growth and transport. Tau's function and stability are modulated by phosphorylation at multiple sites [60, 61]. Deletion of Tau leads to age-dependent short-term memory deficits, hyperactivity, and synaptic plasticity defects [62]. Hyperphosphorylation of Tau results in the formation of neurofibrillary tangles, a hallmark of AD pathology [63]. APOE isoforms have been shown to modulate Tau phosphorylation and aggregation in an isoform-dependent manner, with APOE4 being particularly associated with increased Tau pathology [64]. Based on these findings, we investigated levels of total Tau and various phosphorylated Tau species (pS^{202}, pT^{231}, and $pS^{396-404}$) in the brains of $APOE2^{hA\beta}$, $APOE3^{hA\beta}$, and $APOE4^{hA\beta}$ rats (Fig. 4a). Total Tau levels were higher in $Apoe^{hA\beta}$ males compared to $APOE2^{hA\beta}$, $APOE3^{hA\beta}$ and $APOE4^{hA\beta}$ males while in females, only $APOE4^{hA\beta}$ rats showed lower Tau levels compared to $Apoe^{hA\beta}$ females (Fig. 4b; Statistical analysis is in Table 3). However, there were no differences in phosphorylated Tau at pS^{202} and pT^{231} across any of the groups (Fig. 4c and d; Statistical

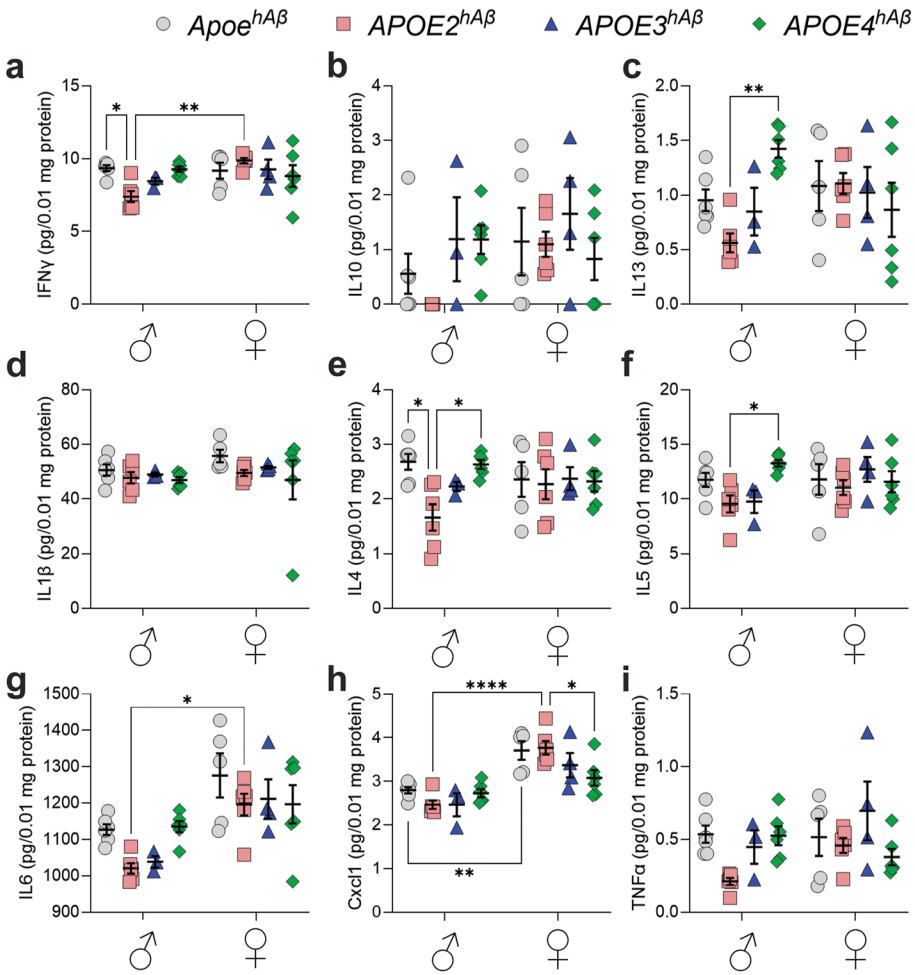

Fig. 5 Levels of cytokines in *Apoe*$^{hA\beta}$, *APOE2*$^{hA\beta}$, *APOE3*$^{hA\beta}$ and *APOE4*$^{hA\beta}$ rats' brains. ELISA measurements for IFN-γ (**a**), IL10 (**b**), IL13 (**c**), IL-1β (**d**), IL-4 (**e**), IL-5 (**f**), IL-6 (**g**), Cxcl1 (**h**), and TNF-α (**i**) were conducted on the same brain homogenates used in Fig. 3a-i (n=3-6 per sex per genotype). Data are represented as mean ± SEM and were analyzed by two-way ANOVA followed by post-hoc Tukey's multiple comparisons tests when ANOVA showed significant differences. Statistical significance is denoted as * p<0.05, ** p<0.01, *** p<0.001, **** p<0.0001

analysis is in Table 3). For pS$^{396\text{-}404}$, phosphorylated Tau levels were lower in *APOE4*$^{hA\beta}$ males compared to *Apoe*$^{hA\beta}$ males, but no differences were observed in females (Fig. 4e; Statistical analysis is in Table 3).

These findings indicate that the observed differences in Tau levels are specific to the comparison between *Apoe*$^{hA\beta}$ and humanized APOE variants with no significant differences detected among the human APOE isoforms.

Sex- and APOE isoform-dependent variations in the brain cytokine levels

APOE isoforms are known to differentially influence the innate immune response [65]. Epidemiological study suggests that non-steroidal anti-inflammatory drugs (NSAIDs) may reduce AD risk, particularly in *APOE4* carriers [66]. Impaired APOE4 function has also been linked to modulation of Aβ-induced neuroinflammation [67]. Thus, we investigated neuroinflammation in the brain of *APOE2*$^{hA\beta,}$ *APOE3*$^{hA\beta}$ and *APOE4*$^{hA\beta}$ rats. Male *APOE2*$^{hA\beta}$ rats exhibited significantly lower Interferon γ (IFNγ) levels compared to *Apoe*$^{hA\beta}$ males and *APOE2*$^{hA\beta}$ females (Fig. 5a; Statistical analysis is in Table 4). There was no significant difference in IL10, IL1β and TNFα levels across the humanized APOE variants (Fig. 5b, d, i). Male *APOE2*$^{hA\beta}$ rats displayed significantly lower levels of anti-inflammatory cytokines of IL13, IL5 and IL4 compared to *APOE4*$^{hA\beta}$ males, while no significant differences were observed in female rats (Fig. 5c, e, f; Statistical analysis is in Table 4). Additionally, male *APOE2*$^{hA\beta}$ rats showed lower IL4 levels compared to *Apoe*$^{hA\beta}$ males. IL6 levels were significantly higher in female *APOE2*$^{hA\beta}$ rats compared to male *APOE2*$^{hA\beta}$ rats (Fig. 5g; Statistical analysis is in Table 4). *APOE2*$^{hA\beta}$ females exhibited higher

Table 4 Statistical analysis results of Fig. 5

			IFNγ	IL10	IL13	IL1β	IL4	IL5	IL6	Cxcl1	TNFα
Two-way ANOVA summary	Sex-genotype interaction	$F_{(3,34)}$=	4.947	1.293	4.419	0.2177	2.272	2/367	1.143	3.366	2.679
		p	0.0059	0.2926	0.010	0.8835	0.0979	0.0881	0.3459	0.0297	0.0625
	Sex factor	$F_{(1,34)}$=	4.077	2.369	0.3705	0.9967	0.0327	1.181	27.45	54.93	1.703
		p	0.0514	0.1331	0.5468	0.3252	0.8574	0.2848	<0.0001	<0.0001	0.2007
	Genotype factor	$F_{(3,34)}$=	0.7665	1.395	1.423	1.364	2.962	2.437	2.693	2.158	2.747
		p	0.5208	0.2612	0.2530	0.2704	0.0459	0.0815	0.0615	0.1111	0.0580
Post hoc Tukey's Analysis: *p*-Values for Multiple Comparisons											
♂:*Apoe*^{hAβ}vs.♂:*APOE2*^{hAβ}			0.0424	0.9618	0.6264	0.9977	0.0244	0.5510	0.3796	0.7734	0.1159
♂:*Apoe*^{hAβ} vs.♂:*APOE3*^{hAβ}			0.9170	0.9749	>0.9999	>0.9999	0.8996	0.8435	0.8077	0.9007	0.9982
♂:*Apoe*^{hAβ} vs. ♂:*APOE4*^{hAβ}			>0.9999	0.9314	0.3991	0.9895	>0.9999	0.8838	>0.9999	>0.9999	>0.9999
♂:*Apoe*^{hAβ} vs. ♀:*Apoe*^{hAβ}			>0.9999	0.9606	0.9990	0.9489	0.9585	>0.9999	0.0970	0.0056	>0.9999
♂:*Apoe*^{hAβ} vs. ♀:*APOE2*^{hAβ}			0.9862	0.9683	0.9964	>0.9999	0.8400	0.9981	0.8389	0.0014	0.9971
♂:*Apoe*^{hAβ} vs. ♀:*APOE3*^{hAβ}			>0.9999	0.5901	>0.9999	>0.9999	0.9771	0.9950	0.7676	0.2695	0.9072
♂:*Apoe*^{hAβ} vs. ♀:*APOE4*^{hAβ}			0.9820	0.9995	>0.9999	0.9906	0.9132	>0.9999	0.8321	0.8814	0.8592
♂:*APOE2*^{hAβ}vs. ♂:*APOE3*^{hAβ}			0.8218	0.6005	0.9578	>0.9999	0.7502	>0.9999	>0.9999	>0.9999	0.6879
♂:*APOE2*^{hAβ} vs.♂:*APOE4*^{hAβ}			0.0570	0.3561	0.0078	>0.9999	0.0371	0.0488	0.2897	0.9190	0.1393
♂:*APOE2*^{hAβ} vs. ♀:*Apoe*^{hAβ}			0.1130	0.4555	0.3311	0.6647	0.3299	0.5895	0.0004	<0.0001	0.2132
♂:*APOE2*^{hAβ}vs.♀:*APOE2*^{hAβ}			0.0043	0.4513	0.2302	0.9999	0.4362	0.8992	0.0189	<0.0001	0.3917
♂:*APOE2*^{hAβ} vs.♀:*APOE3*^{hAβ}			0.1240	0.1294	0.5609	0.9929	0.3825	0.2505	0.0240	0.0120	0.0116
♂:*APOE2*^{hAβ} vs.♀:*APOE4*^{hAβ}			0.2845	0.7673	0.8536	>0.9999	0.3332	0.6513	0.0183	0.1083	0.8183
♂:*APOE3*^{hAβ} vs.♂:*APOE4*^{hAβ}			0.9460	>0.9999	0.4018	>0.9999	0.9424	0.2313	0.7301	0.9699	0.9992
♂:*APOE3*^{hAβ} vs. ♀:*Apoe*^{hAβ}			0.9773	>0.9999	0.9883	0.9199	>0.9999	0.8531	0.0098	0.0012	0.9998
♂:*APOE3*^{hAβ} vs.♀:*APOE2*^{hAβ}			0.5301	>0.9999	0.9764	>0.9999	>0.9999	0.9841	0.1723	0.0004	>0.9999
♂:*APOE3*^{hAβ} vs.♀:*APOE3*^{hAβ}			0.9666	0.9975	0.9985	0.9998	>0.9999	0.5375	0.1572	0.0509	0.7200
♂:*APOE3*^{hAβ} vs.♀:*APOE4*^{hAβ}			0.9997	0.9991	>0.9999	>0.9999	>0.9999	0.8970	0.1685	0.2913	0.9996
♂:*APOE4*^{hAβ} vs. ♀:*Apoe*^{hAβ}			>0.9999	>0.9999	0.8076	0.5514	0.9831	0.9164	0.1367	0.0023	>0.9999
♂:*APOE4*^{hAβ} vs.♀:*APOE2*^{hAβ}			0.9707	>0.9999	0.8230	0.9987	0.9093	0.5250	0.9087	0.0006	0.9988
♂:*APOE4*^{hAβ} vs.♀:*APOE3*^{hAβ}			>0.9999	0.9923	0.7230	0.9783	0.9915	0.9998	0.8460	0.1562	0.8772
♂:*APOE4*^{hAβ} vs.♀:*APOE4*^{hAβ}			0.9924	0.9972	0.2045	>0.9999	0.9585	0.8125	0.9038	0.7128	0.8953
♀:*Apoe*^{hAβ} vs. ♀:*APOE2*^{hAβ}			0.9483	>0.9999	>0.9999	0.8760	>0.9999	0.9981	0.7621	>0.9999	0.9997
♀:*Apoe*^{hAβ} vs. ♀:*APOE3*^{hAβ}			>0.9999	0.9903	>0.9999	0.9912	>0.9999	0.9969	0.9421	0.8656	0.8637
♀:*Apoe*^{hAβ} vs. ♀:*APOE4*^{hAβ}			0.9987	0.9990	0.9778	0.5610	>0.9999	>0.9999	0.7697	0.1245	0.9427
♀:*APOE2*^{hAβ} vs.♀:*APOE3*^{hAβ}			0.9823	0.9793	>0.9999	0.9999	>0.9999	0.8909	>0.9999	0.6998	0.5832
♀:*APOE2*^{hAβ} vs.♀:*APOE4*^{hAβ}			0.6261	0.9995	0.9514	0.9989	>0.9999	0.9997	>0.9999	0.0482	0.9963
♀:*APOE3*^{hAβ} vs.♀:*APOE4*^{hAβ}			0.9967	0.8520	0.9977	0.9801	>0.9999	0.9861	>0.9999	0.9201	0.2316

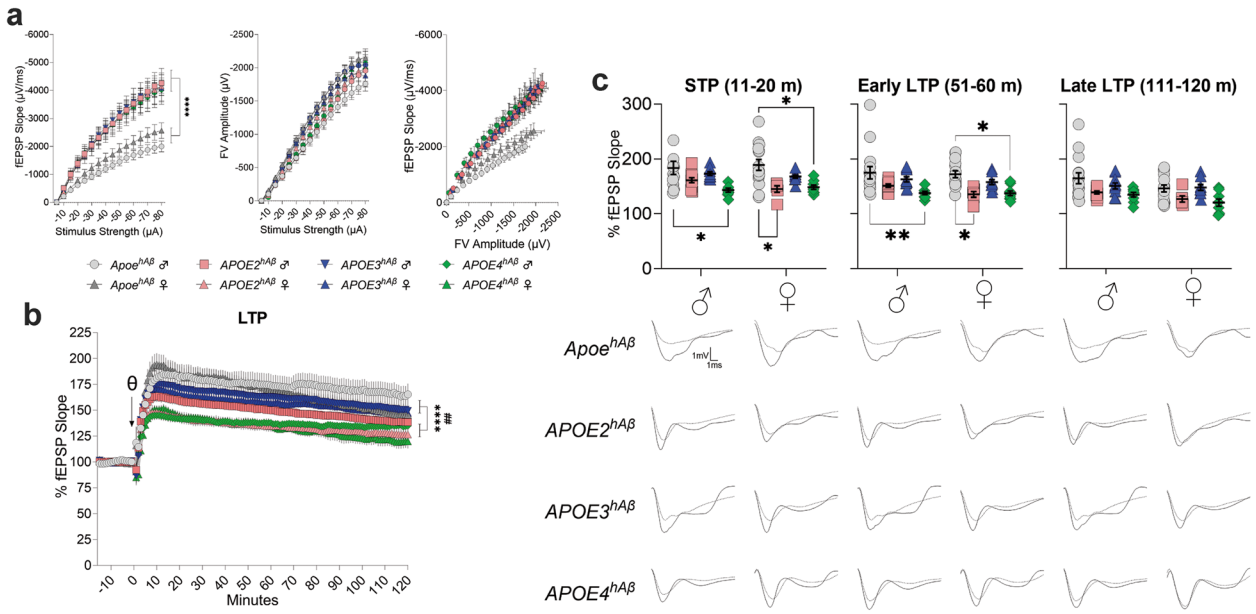

Fig. 6 Effects of APOE variants on synaptic transmission and plasticity. **a** IO recording of APOE variants in hippocampal Schafer Colleterals-CA1 circuit. Left panel, I-O curve generated from the slope fEPSP versus stimulus strength. Middle panel, I-O curve generated from FV amplitude versus stimulus strength. Right panel, I-O curve generated from the slope fEPSP versus FV amplitude. Each genotype/sex is compared separately. Data is represented as mean ± SEM. Data were analyzed by two-way ANOVA (Column factor). See the statistical analysis in Table 5. **b** LTP Recordings in the Hippocampal Schaffer Collateral-CA1 Circuit of 80-Day-Old APOE Variant Rats. LTP recordings are weaker in both male and female *APOE2*$^{hA\beta}$ and *APOE4*$^{hA\beta}$ rats compared to *Apoe*$^{hA\beta}$and *APOE3*$^{hA\beta}$ rats. Each genotype/sex is compared separately. Data are represented as mean ± SEM. Data were analyzed by two-way ANOVA. See Table 5 for statistical analysis. **c** Plot of fEPSP slope change in STP (11-20 m), early LTP (51-60 m) and late LTP (111-120 m) phases of LTP. The average traces of the baseline (dotted line) and STP, early LTP and late LTP (solid line) are shown on bottom. Data are represented as mean ± SEM. Data were analyzed by two-way ANOVA for repeated measures followed by *post-hoc* Tukey's multiple comparisons test when ANOVA showed statistically significant differences. Statistical analysis are shown in Table 6

Cxcl1 levels than both *APOE4*$^{hA\beta}$ females and *APOE2*$^{hA\beta}$ males. Additionally, *Apoe*$^{hA\beta}$ females showed significantly higher levels compared to *Apoe*$^{hA\beta}$ males (Fig. 5h; Statistical analysis is in Table 4).

In conclusion, *APOE2*$^{hA\beta}$ males exhibited lower levels of cytokines, while variations in cytokine levels among females were less pronounced, suggesting a distinct influence of APOE isoforms on neuroinflammation, particularly in males.

APOE isoform-dependent impairment in synaptic plasticity

LTP is a long-lasting form of synaptic plasticity and is widely recognized as the cellular basis of memory. Given the LTP deficits observed in *Apoe*-deficient mice [68], we measured I/O and LTP responses to assess the effects of APOE variants on synaptic plasticity in the Schafer collateral-CA1 circuit using hippocampal slices from humanized *APOE* variant-carrying rats. Before recording LTP, we examined the slope of field excitatory postsynaptic potentiation (fEPSP) evoked by increasing current stimulation. Both male and female *APOE2*$^{hA\beta}$, *APOE3*$^{hA\beta}$ and *APOE4*$^{hA\beta}$ rats exhibited an increased fEPSP slope in I/O responses compared same-sex *Apoe*$^{hA\beta}$ rats, suggesting heightened excitability across all humanized APOE rats (Fig. 6a-left panel; Statistical analysis is in Table 5). Moreover, the amplitudes of fiber volley (FV), which reflects the size of ascending fiber stimulus, were higher in male *APOE2*$^{hA\beta}$ and *APOE3*$^{hA\beta}$ rats compared to *Apoe*$^{hA\beta}$ males, while no differences were observed among females (Fig. 6a-middle panel; Statistical analysis is in Table 5). Additionally, FV amplitude versus evoked fEPSP slope were also analyzed, showing that *Apoe*$^{hA\beta}$ rats were distinct from all humanized APOE-carrying rats, while humanized APOE groups were indistinguishable (Fig. 6a-right panel).

After I/O recordings, we examined LTP elicited by Θ-burst stimulation. Prior to induction, baseline recordings were taken for 15 mins using an intensity that elicited 40% of the maximum response observed in the I/O recordings. We observed a reduction in the whole LTP curve analysis in both male and female *APOE4*$^{hA\beta}$ rats compared to same-sex *Apoe*$^{hA\beta}$ and *APOE3*$^{hA\beta}$ rats. Additionally, both male and female *APOE2*$^{hA\beta}$ rats showed reduced LTP compared to same-sex *APOE3*$^{hA\beta}$ rats, with female *APOE2*$^{hA\beta}$ rats also exhibiting LTP deficit compared to *Apoe*$^{hA\beta}$ females

Table 5 Statistical analysis results of Fig. 6

Two-way ANOVA summary		IO-fEPSP	IO-FV	LTP
♂:$Apoe^{hA\beta}$vs.♂:$APOE2^{hA\beta}$	$F_{(1,33)=}$	32.24	9.947	3.289
	p	<0.0001	0.0036	0.0828
♂:$Apoe^{hA\beta}$ vs.♂:$APOE3^{hA\beta}$	$F_{(1,35)=}$	37.24	8.994	0.8056
	p	<0.0001	0.0051	0.3787
♂:$Apoe^{hA\beta}$ vs. ♂:$APOE4^{hA\beta}$	$F_{(1,33)=}$	27.13	0.676	6.819
	p	<0.0001	0.4172	0.0159
♂:$APOE2^{hA\beta}$vs. ♂:$APOE3^{hA\beta}$	$F_{(1,20)=}$	0.0026	0.1508	4.788
	p	0.9598	0.7019	0.0421
♂:$APOE2^{hA\beta}$ vs.♂:$APOE4^{hA\beta}$	$F_{(1,18)=}$	0.0802	3.764	8.752
	p	0.7802	0.0682	0.0088
♂:$APOE3^{hA\beta}$ vs.♂:$APOE4^{hA\beta}$	$F_{(1,18)=}$	0.122	2.969	20.20
	p	0.7305	0.1003	0.0003
♀:$Apoe^{hA\beta}$ vs. ♀:$APOE2^{hA\beta}$	$F_{(1,23)=}$	6.278	0.2425	8.265
	p	0.0197	0.6271	0.0097
♀:$Apoe^{hA\beta}$ vs. ♀:$APOE3^{hA\beta}$	$F_{(1,33)=}$	35.75	0.8018	1.323
	p	<0.0001	0.3791	0.2623
♀:$Apoe^{hA\beta}$ vs. ♀:$APOE4^{hA\beta}$	$F_{(1,25)=}$	8.307	1.131	13.79
	p	0.008	0.2976	0.0012
♀:$APOE2^{hA\beta}$ vs.♀:$APOE3^{hA\beta}$	$F_{(1,16)=}$	0.0003	0.082	11.62
	p	0.9846	0.7783	0.0047
♀:$APOE2^{hA\beta}$ vs.♀:$APOE4^{hA\beta}$	$F_{(1,16)=}$	0.0007	0.2130	0.1034
	p	0.9781	0.6506	0.7529
♀:$APOE3^{hA\beta}$ vs.♀:$APOE4^{hA\beta}$	$F_{(1,16)=}$	0.0002	0.0925	18.95
	p	0.9870	0.7575	0.0005

(Fig. 6b; Statistical analysis is in Table 5). We then analyzed LTP's three different phases: STP, early LTP and late LTP. Both STP and early LTP were reduced in male and female $APOE4^{hA\beta}$ rats compared to same-sex $Apoe^{hA\beta}$ rats. Additionally, female $APOE2^{hA\beta}$ rats exhibited reduced STP and early LTP compared to $Apoe^{hA\beta}$ females (Fig. 6c; Statistical analysis is in Table 5). For late LTP, although $APOE4^{hA\beta}$ rats showed lower levels than $Apoe^{hA\beta}$ rats, the difference did not reach statistical significance. These findings suggest that APOE isoforms, particularly APOE4 and to a lesser extent APOE2, impair synaptic plasticity, with significant deficits in both STP and early LTP, highlighting the critical role of APOE in modulating synaptic function and memory processes.

Increased triglyceride and cholesterol levels in $APOE2^{hA\beta}$ rats

Next, we measured blood glucose, triglyceride, cholesterol, LDL and HDL levels using home test kits while collecting blood via cardiac puncture, to assess the metabolic health of our rats after a 16-hour fasting period. No significant variance was observed in the levels of blood glucose (Fig. 7a; Statistical analysis is in Table 7). In contrast, both blood triglyceride (Fig. 7b) and cholesterol levels (Fig. 7c) were significantly higher in $APOE2^{hA\beta}$ compared to $Apoe^{hA\beta}$, $APOE3^{hA\beta}$ and $APOE4^{hA\beta}$ rats (Statistical analysis is in Table 7). In addition, the serum of $APOE2^{hA\beta}$ rats exhibited a turbid appearance (Fig. 7g) reminiscent of human cases of type III HLP [35]. This observation, coupled with evident mixed hypercholesterolemia and hypertriglyceridemia, supports the characterization of $APOE2^{hA\beta}$ rats as a model for type III HLP, a condition prevalent in a significant fraction of individuals homozygous for APOE2 [30, 36–39].

HDL levels were similar in all humanized *APOE* groups, but lower compared to $Apoe^{hA\beta}$ group (Fig. 7d; Statistical analysis is in Table 7). Moreover, the level of LDL is similar in all humanized *APOE* groups. But LDL levels were higher in $APOE2^{hA\beta}$ rats compared to $Apoe^{hA\beta}$ (Fig. 7e; Statistical analysis is in Table 7). As a result, the LDL/HDL ratio was much higher in male $APOE2^{hA\beta}$ compared to male $Apoe^{hA\beta}$ and $APOE3^{hA\beta}$ rats, but there was no difference between groups in females (Fig. 7f; Statistical analysis is in Table 7). The LDL/HDL ratio is used to predict Coronary Heart Disease (CHD), with a higher ratio indicating a higher risk of CHD [69].

Sex- and APOE isoform-dependent variations in serum lipidomics

A comprehensive lipidomic analysis was conducted to measure 222 lipid molecular species in serum samples of $Apoe^{hA\beta}$, $APOE2^{hA\beta}$, $APOE3^{hA\beta}$ and $APOE4^{hA\beta}$ rats, after scanning thousands of lipid molecular species. The lipid species included 3 phosphatidylglycerol (PG) species, 3 phosphatidylserine (PS) species, 21 phosphatidylethanolamine (PE) species, 13 plasmalogen PE (pPE) species, 12 lyso PE (LPE) species, 11 acylcarnitine (CAR) species, 6 phosphatidylinositol (PI) species, 20 sphingomyelin (SM) species, 31 phosphatidylcholine (PC) species, 4 plasmalogen PC (pPC) species, 12 lyso PC (LPC) species, 59 types of triacylglycerol (TAG) without deconvolution of individual molecular species, 11 types of fatty acyl chains in TAG (FA), total cholesterol, free cholesterol, and 14 types of cholesterol esters.

The results revealed significant differences in levels of various lipid molecular species between the different *APOE* genotypes. Notably, $APOE2^{hA\beta}$ rats displayed markedly elevated levels of serum PG, PS, PE, pPE, SM, LPC, TAG, FA, total cholesterol, free cholesterol, and cholesterol esters compared to $Apoe^{hA\beta}$, $APOE3^{hA\beta}$, and $APOE4^{hA\beta}$ rats in both males and females (Fig. 8a-d, h, k-p; see Table 8 for statistical analysis results). The levels of LPE, CAR, PI, and PC showed sex-dependent variations in $Apoe^{hA\beta}$ rats (Fig. 8e-g, i-j; Statistical analysis is

Table 6 Statistical analysis results of three phases of LTP

			STP	E-LTP	L-LTP
Two-way ANOVA summary	Sex-genotype interaction	$F_{(3,75)}$=	0.6272	0.3377	0.4729
		p	0.5997	0.7981	0.7021
	Sex factor	$F_{(1,75)}$=	0.1878	1.27	5.195
		p	0.666	0.2633	0.0255
	Genotype factor	$F_{(3,75)}$=	9.641	10.89	7.032
		p	<0.0001	<0.0001	0.0003
Post hoc Tukey's Analysis: *p*-Values for Multiple Comparisons					
♂:*Apoe*$^{hA\beta}$vs.♂:*APOE2*$^{hA\beta}$			0.5155	0.2179	0.1188
♂:*Apoe*$^{hA\beta}$ vs.♂:*APOE3*$^{hA\beta}$			0.9843	0.9153	0.8047
♂:*Apoe*$^{hA\beta}$ vs. ♂:*APOE4*$^{hA\beta}$			0.0200	0.0080	0.0515
♂:*Apoe*$^{hA\beta}$ vs. ♀:*Apoe*$^{hA\beta}$			0.9994	>0.9999	0.3406
♂:*Apoe*$^{hA\beta}$ vs. ♀:*APOE2*$^{hA\beta}$			0.0938	0.0179	0.0223
♂:*Apoe*$^{hA\beta}$ vs. ♀:*APOE3*$^{hA\beta}$			0.8806	0.6648	0.6551
♂:*Apoe*$^{hA\beta}$ vs. ♀:*APOE4*$^{hA\beta}$			0.0675	0.0069	0.0005
♂:*APOE2*$^{hA\beta}$vs. ♂:*APOE3*$^{hA\beta}$			0.9787	0.9477	0.9412
♂:*APOE2*$^{hA\beta}$ vs.♂:*APOE4*$^{hA\beta}$			0.8447	0.9197	>0.9999
♂:*APOE2*$^{hA\beta}$ vs. ♀:*Apoe*$^{hA\beta}$			0.2371	0.3681	0.9944
♂:*APOE2*$^{hA\beta}$vs.♀:*APOE2*$^{hA\beta}$			0.9470	0.8982	0.9732
♂:*APOE2*$^{hA\beta}$ vs.♀:*APOE3*$^{hA\beta}$			0.9996	0.9986	0.9891
♂:*APOE2*$^{hA\beta}$ vs.♀:*APOE4*$^{hA\beta}$			0.9709	0.9066	0.6592
♂:*APOE3*$^{hA\beta}$ vs.♂:*APOE4*$^{hA\beta}$			0.2793	0.2898	0.7956
♂:*APOE3*$^{hA\beta}$ vs. ♀:*Apoe*$^{hA\beta}$			0.8582	0.9795	0.9996
♂:*APOE3*$^{hA\beta}$ vs.♀:*APOE2*$^{hA\beta}$			0.5120	0.3214	0.4876
♂:*APOE3*$^{hA\beta}$ vs.♀:*APOE3*$^{hA\beta}$			0.9999	0.9997	>0.9999
♂:*APOE3*$^{hA\beta}$ vs.♀:*APOE4*$^{hA\beta}$			0.5238	0.2700	0.0936
♂:*APOE4*$^{hA\beta}$ vs. ♀:*Apoe*$^{hA\beta}$			0.0047	0.0189	0.9387
♂:*APOE4*$^{hA\beta}$ vs.♀:*APOE2*$^{hA\beta}$			>0.9999	>0.9999	0.9982
♂:*APOE4*$^{hA\beta}$ vs.♀:*APOE3*$^{hA\beta}$			0.5660	0.6213	0.9254
♂:*APOE4*$^{hA\beta}$ vs.♀:*APOE4*$^{hA\beta}$			>0.9999	>0.9999	0.8890
♀:*Apoe*$^{hA\beta}$ vs. ♀:*APOE2*$^{hA\beta}$			0.0325	0.0363	0.6775
♀:*Apoe*$^{hA\beta}$ vs. ♀:*APOE3*$^{hA\beta}$			0.6178	0.8299	>0.9999
♀:*Apoe*$^{hA\beta}$ vs. ♀:*APOE4*$^{hA\beta}$			0.0187	0.0167	0.1579
♀:*APOE2*$^{hA\beta}$ vs.♀:*APOE3*$^{hA\beta}$			0.7731	0.6187	0.6719
♀:*APOE2*$^{hA\beta}$ vs.♀:*APOE4*$^{hA\beta}$			>0.9999	>0.9999	0.9994
♀:*APOE3*$^{hA\beta}$ vs.♀:*APOE4*$^{hA\beta}$			0.8116	0.5959	0.1983

in Table 8). In male rats, the levels of these lipid species were lower compared to female rats. Moreover, within the *APOE2*$^{hA\beta}$ rats, males exhibited lower levels of PI compared to females (Fig. 8). Furthermore, a comparison among the humanized *APOE* genotypes revealed additional insights. Female *APOE3*$^{hA\beta}$ and *APOE4*$^{hA\beta}$ rats exhibited lower levels of LPE and CAR compared to female *APOE2*$^{hA\beta}$ rats. Additionally, male *APOE2*$^{hA\beta}$ rats displayed higher levels of LPE compared to male *Apoe*$^{hA\beta}$ and *APOE4*$^{hA\beta}$ rats, and higher levels of CAR compared to male *APOE4*$^{hA\beta}$ rats (Fig. 8). In *APOE3*$^{hA\beta}$ and *APOE4*$^{hA\beta}$ rats, females showed reduced levels of PI, PC, and pPC compared to *Apoe*$^{hA\beta}$ and *APOE2*$^{hA\beta}$ rats of the same sex. Additionally, male *APOE3*$^{hA\beta}$ and *APOE4*$^{hA\beta}$ rats had lower levels of PI compared to male *APOE2*$^{hA\beta}$ rats, with male *APOE4*$^{hA\beta}$ rats also displaying lower levels of PI compared to male *Apoe*$^{hA\beta}$. Moreover, male *APOE2*$^{hA\beta}$ rats exhibited higher levels of PC, pPC, and LPC compared to male *Apoe*$^{hA\beta}$, *APOE3*$^{hA\beta}$, and *APOE4*$^{hA\beta}$ rats (Fig. 8).

We also analyzed the ratios of TAG to PC and FA 18:1 to FA 18:2 which are indicators of the size of lipoproteins and FA profiles in TAG pools, respectively, since FA 18:1 largely represents the de novo synthesized pool

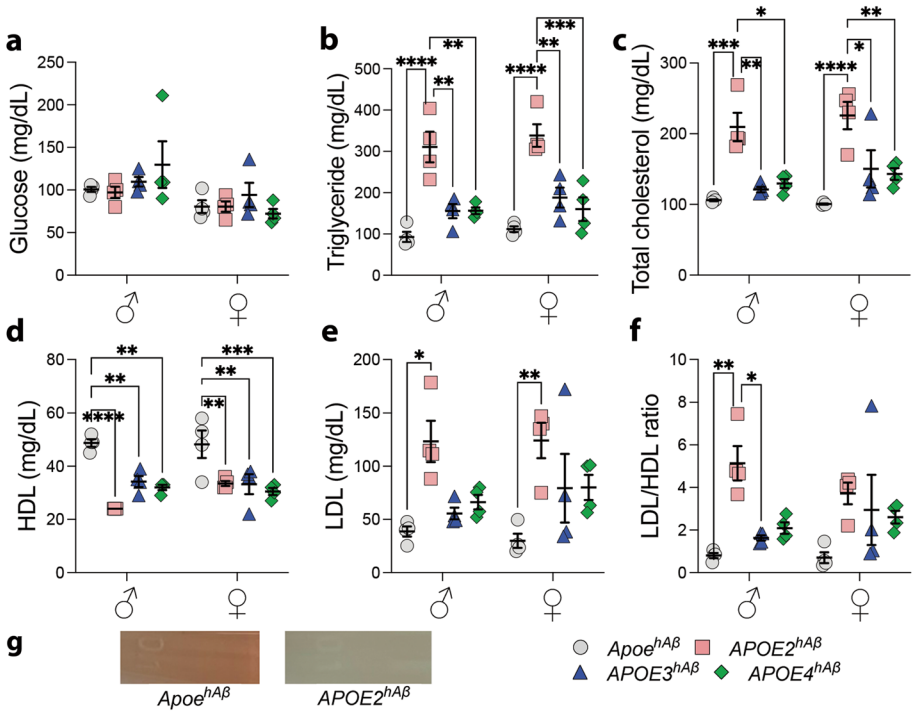

Fig. 7 Metabolic profiles in 80-day-old rats: blood glucose, lipids, and LDL/HDL ratio after fasting. *Apoe*$^{hA\beta}$, *APOE2*$^{hA\beta}$, *APOE3*$^{hA\beta}$ and *APOE4*$^{hA\beta}$ rats (n=4 per sex per genotype) were analyzed for blood levels of glucose (**a**), triglycerides (**b**), total cholesterol (**c**), HDL (**d**), LDL (**e**) and for LDL/HDL ratio (**f**). **g** The serum of *APOE2*$^{hA\beta}$ rats exhibited a turbid appearance reminiscent of human cases of type III HLP. Data are represented as mean ± SEM and were analyzed by two-way ANOVA followed by post hoc Tukey's multiple comparisons test when ANOVA showed a significant difference. When the measurements were discovered to exceed the range, the nearest integer beyond the range was assigned. Statistical significance is denoted as * p<0.05, ** p<0.01, *** p<0.001, **** p<0.0001

and FA 18:2 represents the portion from dietary uptake. *APOE2*$^{hA\beta}$ rats have much higher TAG/PC ratio compared to all other variants in male animals, indicating a relatively larger size of lipoprotein particles in *APOE2*$^{hA\beta}$ male rats compared to the other counterparts (Fig. 8q; Statistical analysis is in Table 8). But, in females TAG/PC ratio was higher in both *APOE2*$^{hA\beta}$ and *APOE3*$^{hA\beta}$ compared to *Apoe*$^{hA\beta}$ rats (Fig. 8q). Moreover, FA18:1/FA 18:2 ratio was lower in male *Apoe*$^{hA\beta}$ rats compared to females (Fig. 8r; Statistical analysis is in Table 8). Also, FA18:1/FA 18:2 ratio was lower in *APOE4*$^{hA\beta}$ compared to *Apoe*$^{hA\beta}$ in both sexes. A lower FA18:1/FA 18:2 ratio was manifest in *APOE2*$^{hA\beta}$ and *APOE3*$^{hA\beta}$ females compared to *Apoe*$^{hA\beta}$ animals (Fig. 8r). These different FA ratios clearly indicate the different lipid metabolism at the FA levels.

Given the markedly elevated lipid levels in *APOE2*$^{hA\beta}$ relative to other variants, it becomes impractical to compare lipid changes among *Apoe*$^{hA\beta}$, *APOE3*$^{hA\beta}$, and *APOE4*$^{hA\beta}$. Consequently, in Fig. 9, we have selectively excluded the *APOE2*$^{hA\beta}$ rats, thereby replicating the analytical approach employed in Fig. 8 without incorporating the *APOE2*$^{hA\beta}$ dataset. First, we observed that both sexes of *APOE4*$^{hA\beta}$ rats had lower levels of PG compared to *APOE3*$^{hA\beta}$ rats (Fig. 9a; Statistical analysis is in Table 9).

In male *Apoe*$^{hA\beta}$ animals, the levels of PE, pPE, LPE, CAR, PI, PC, total cholesterol, and free cholesterol were found to be lower compared to their female counterparts. In *APOE4*$^{hA\beta}$ animals, females exhibited lower levels of PE, pPE, LPE, CAR, PI, SM, PC, pPC, LPC, total cholesterol, free cholesterol, cholesterol esters, and the ratio of FA18:1/FA18:2 when compared to female *Apoe*$^{hA\beta}$ animals (Fig. 9c-k, n-p, r; see Table 9 for statistical analysis results). Similarly, male *APOE4*$^{hA\beta}$ rats had lower levels of PI, SM, pPC, LPC, total cholesterol, and cholesterol esters compared to male *Apoe*$^{hA\beta}$ rats. Additionally, female *APOE3*$^{hA\beta}$ rats showed lower levels of pPE, CAR, PI, SM, PC, pPC, LPC, total cholesterol, free cholesterol, cholesterol esters and ratio of FA18:1/FA18:2 compared to female *Apoe*$^{hA\beta}$ rats. Conversely, female *APOE3*$^{hA\beta}$ rats showed a higher ratio of TAG to PC (Fig. 9q). Male *APOE3*$^{hA\beta}$ rats, on the other hand, only had lower levels of SM compared to male *Apoe*$^{hA\beta}$ animals. PS, TAG and FA levels were comparable in *Apoe*$^{hA\beta}$, *APOE3*$^{hA\beta}$ and *APOE4*$^{hA\beta}$ (Fig. 9b, l-m; Statistical analysis is in Table 9).

Table 7 Statistical analysis results of Fig. 7

			Glucose	Triglyceride	Total Chol.	HDL	LDL	LDL/HDL
Two-way ANOVA summary	Sex-genotype interaction	$F_{(3,24)}$=	1.389	0.1583	0.5164	2.178	0.4133	1.372
		p	0.2701	0.9233	0.6749	0.1168	0.7450	0.2752
	Sex factor	$F_{(1,24)}$=	10.40	1.697	1.798	0.8298	0.4476	0.02442
		p	0.0036	0.2051	0.1925	0.3714	0.5098	0.8771
	Genotype factor	$F_{(3,24)}$=	0.6423	35.47	23.93	24.69	11.07	9385
		p	0.5953	<0.0001	<0.0001	<0.0001	<0.0001	0.0003
Post hoc Tukey's Analysis: *p*-Values for Multiple Comparisons								
♂:$Apoe^{hA\beta}$vs.♂:$APOE2^{hA\beta}$			>0.9999	<0.0001	0.0006	<0.0001	0.0163	0.0040
♂:$Apoe^{hA\beta}$ vs.♂:$APOE3^{hA\beta}$			0.9994	0.5244	0.9941	0.0090	0.9936	0.9890
♂:$Apoe^{hA\beta}$ vs. ♂:$APOE4^{hA\beta}$			0.6869	0.5100	0.9306	0.0020	0.9114	0.8875
♂:$Apoe^{hA\beta}$ vs. ♀:$Apoe^{hA\beta}$			0.9278	0.9986	>0.9999	>0.9999	>0.9999	>0.9999
♂:$Apoe^{hA\beta}$ vs. ♀:$APOE2^{hA\beta}$			0.9278	<0.0001	<0.0001	0.0055	0.0149	0.1040
♂:$Apoe^{hA\beta}$ vs. ♀:$APOE3^{hA\beta}$			>0.9999	0.0981	0.3762	0.0046	0.6074	0.4003
♂:$Apoe^{hA\beta}$ vs. ♀:$APOE4^{hA\beta}$			0.7044	0.4399	0.5920	0.0007	0.5850	0.6108
♂:$APOE2^{hA\beta}$vs. ♂:$APOE3^{hA\beta}$			0.9950	0.0013	0.0037	0.1232	0.0871	0.0288
♂:$APOE2^{hA\beta}$ vs.♂:$APOE4^{hA\beta}$			0.5601	0.0014	0.0102	0.3633	0.2150	0.0796
♂:$APOE2^{hA\beta}$ vs. ♀:$Apoe^{hA\beta}$			0.9727	<0.0001	0.0003	<0.0001	0.0064	0.0031
♂:$APOE2^{hA\beta}$vs.♀:$APOE2^{hA\beta}$			0.9727	0.9863	0.9905	0.1826	>0.9999	0.8303
♂:$APOE2^{hA\beta}$ vs.♀:$APOE3^{hA\beta}$			>0.9999	0.0155	0.1018	0.2068	0.5139	0.3729
♂:$APOE2^{hA\beta}$ vs.♀:$APOE4^{hA\beta}$			0.8172	0.0019	0.0477	0.6124	0.5361	0.2137
♂:$APOE3^{hA\beta}$ vs.♂:$APOE4^{hA\beta}$			0.9321	>0.9999	0.9998	0.9980	0.9997	0.9997
♂:$APOE3^{hA\beta}$ vs. ♀:$Apoe^{hA\beta}$			0.6780	0.8621	0.9653	0.0125	0.9361	0.9786
♂:$APOE3^{hA\beta}$ vs.♀:$APOE2^{hA\beta}$			0.6780	0.0002	0.0005	>0.9999	0.0802	0.4291
♂:$APOE3^{hA\beta}$ vs.♀:$APOE3^{hA\beta}$			0.9822	0.9658	0.8171	>0.9999	0.9578	0.8751
♂:$APOE3^{hA\beta}$ vs.♀:$APOE4^{hA\beta}$			0.3866	>0.9999	0.9500	0.9609	0.9499	0.9718
♂:$APOE4^{hA\beta}$ vs. ♀:$Apoe^{hA\beta}$			0.1197	0.8519	0.8233	0.0028	0.7256	0.8436
♂:$APOE4^{hA\beta}$ vs.♀:$APOE2^{hA\beta}$			0.1197	0.0002	0.0014	0.9999	0.2003	0.7156
♂:$APOE4^{hA\beta}$ vs.♀:$APOE3^{hA\beta}$			0.4532	0.9698	0.9630	>0.9999	0.9987	0.9864
♂:$APOE4^{hA\beta}$ vs.♀:$APOE4^{hA\beta}$			0.0439	>0.9999	0.9969	0.9999	0.9981	0.9994
♀:$Apoe^{hA\beta}$ vs. ♀:$APOE2^{hA\beta}$			>0.9999	<0.0001	<0.0001	0.0076	0.0058	0.0844
♀:$Apoe^{hA\beta}$ vs. ♀:$APOE3^{hA\beta}$			0.9911	0.2884	0.2449	0.0065	0.3726	0.3447
♀:$Apoe^{hA\beta}$ vs. ♀:$APOE4^{hA\beta}$			0.9996	0.7949	0.4250	0.0010	0.3535	0.5461
♀:$APOE2^{hA\beta}$ vs.♀:$APOE3^{hA\beta}$			0.9911	0.0019	0.0173	>0.9999	0.4893	0.9924
♀:$APOE2^{hA\beta}$ vs.♀:$APOE4^{hA\beta}$			0.9996	0.0002	0.0074	0.9886	0.5112	0.9423
♀:$APOE3^{hA\beta}$ vs.♀:$APOE4^{hA\beta}$			0.8938	0.9848	>0.9999	0.9932	>0.9999	>0.9999

This comprehensive lipidomic analysis across nine lipid classes (CAR, FA, PC, PE, PI, PG, PS, TAG, and SM) revealed distinct patterns of lipid abundance in different rat samples, identified through the generation of heatmaps. Each heatmap provided a color-coded representation of the relative abundance of each lipid type within each sample. Our major finding was that $APOE2^{hA\beta}$ male rats consistently displayed unique lipidomic profiles across all lipid classes. This pattern underscores the substantial influence of genotype on lipid metabolism and suggests that specific genotypes and sex, such as $APOE2^{hA\beta}$ males, might uniquely influence lipid metabolism. This insight has potential implications for understanding disease susceptibilities or responses to treatments in these genetic models.

We observed substantial heterogeneity in lipid composition across samples and lipid species, which underlined the diversity of the lipidomic landscape in the studied rat models. Certain lipid species like PS P-18:0/22:6 and PS O-16:0/22:6 in the PS lipid data, and TAG 48:0 and TAG 50:1 in the TAG lipid data, consistently exhibited lower relative abundances across all samples. These patterns suggest that these lipids might have less dominant role in the overall lipid metabolism, or their functions might be

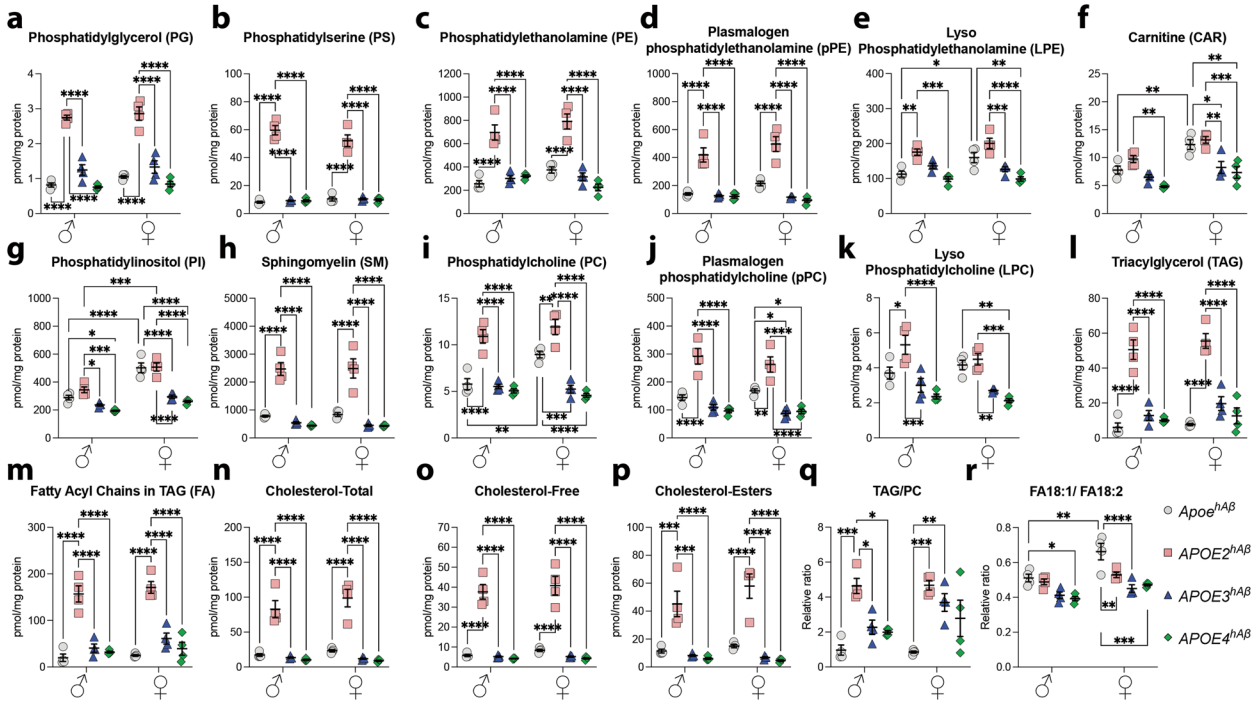

Fig. 8 Serum lipid profile of *Apoe*$^{hA\beta}$, *APOE2*$^{hA\beta}$, *APOE3*$^{hA\beta}$ and *APOE4*$^{hA\beta}$ rats. Levels of PG (**a**), PS (**b**), PE (**c**), pPE (**d**), LPE (**e**), CAR (**f**), PI (**g**), SM (**h**), PC (**i**), pPC (**j**), LPC (**k**), TAG (**l**), FA (**m**), total Cholesterol (**n**), free Cholesterol (**o**) and Cholesterol esters (**p**) and relative ratios of TAG/PC (**q**) and FA18:1/FA 18:2 (**r**) in serum of 80 days old *Apoe*$^{hA\beta}$, *APOE2*$^{hA\beta}$, *APOE3*$^{hA\beta}$ and *APOE4*$^{hA\beta}$ rats are shown (n=4 per sex per genotype). Data are represented as mean ± SEM and were analyzed by two-way ANOVA followed by post hoc Tukey's multiple comparisons test when ANOVA showed a significant difference. Post hoc Tukey's Analysis is shown in Tables 1 and 2. *$p<0.05$, **$p<0.01$, ***$p<0.001$, ****$p<0.0001$

conserved across different rat models. Conversely, certain lipids were found to be consistently present at higher levels across all samples, indicating their prominent role in lipid metabolism across different rat genotypes and sexes. For instance, in the PC lipid data, lipid species such as PC 32:0 and PC 34:1 were observed to have higher relative abundances in most samples (Figs. 10 and 11; All lipid species measurements are listed in Additional file 1).

Correlation heatmaps (Fig. 12) depicted relationships among lipid species in *Apoe*$^{hA\beta}$, *APOE2*$^{hA\beta}$, *APOE3*$^{hA\beta}$, and *APOE4*$^{hA\beta}$ rats. We used the Pearson correlation coefficient to calculate all correlations and p-values between 222 lipid species in each group. We identified the top 20 correlations based on absolute values of correlation coefficients with $p<0.05$. The heatmaps reveal strong positive correlations between different types of lipid species across all groups. The strongest positive correlations were between TAG C52:2/C53:9 and PE D18:0-20:4/D16:0-22:4 in *Apoe*$^{hA\beta}$ rats (r= 0.97), between PE P18:1-20:4/P16:0-22:5 and PE A20:0-20:4/P18:0-22:3 in *APOE2*$^{hA\beta}$ rats (r= 0.98), between CAR 16:2 and CAR 18:2 in *APOE3*$^{hA\beta}$ rats (r= 0.97), between CAR 18:0 and CAR 18:1 in *APOE4*$^{hA\beta}$ rats (r= 0.97). There are strong positive correlations between LPE 20:4 and pPE P18:0-22:6/P18:1-22:5 with correlation coefficients of 0.97, 0.45 and 0.33 in *Apoe*$^{hA\beta}$, *APOE2*$^{hA\beta}$ and *APOE3*$^{hA\beta}$ rats, respectively. Conversely, there are strong negative correlations between CAR 7:0 and PE P16:0-20:3/P18:1-18:2 in *APOE3*$^{hA\beta}$ (r= -0.91) and between SM N18:0 and PE D16:0-20:4/D18:2-18:2 in *APOE4*$^{hA\beta}$ animals (r= -0.94). The heatmaps also show that there are several opposite correlations between the different lipid types in the different groups of animals. A strong positive correlation exists between SM N20:0 and PC D18:0-22:5 with correlation coefficients of 0.76 and 0.32 in *Apoe*$^{hA\beta}$ and *APOE2*$^{hA\beta}$, respectively but in *APOE4*$^{hA\beta}$ animals there is negative correlation (r= -0.55). Similarly, there is a strong negative correlation between PC D18:2-18:2/D16:0-20:4 and SM N24:2 in *APOE4*$^{hA\beta}$ rats with correlation coefficients of -0.68, while there is positive correlation in *Apoe*$^{hA\beta}$ (r= 0.32) and *APOE3*$^{hA\beta}$ rats (r= 0.36). The correlation between CAR 7:0 and CAR 18:1 is more robust in *APOE3*$^{hA\beta}$ rats (r= 0.91) than in *APOE4*$^{hA\beta}$ animals (r= 0.29), suggesting a more pronounced relationship between these two lipid species in *APOE3*$^{hA\beta}$ rats. Another intriguing observation is that the correlation between PE D16:0-22:6 and SM N18:0, while there is strong negative correlation in *APOE4*$^{hA\beta}$ animals (r=

Table 8 Statistical analysis results of Fig. 8

			PG	PS	PE	pPE	LPE	CAR	PI	SM	PC	pPC	LPC	TAG	FA	Chol. Total	Chol. Free	Chol. Esters	TAG/PC	FA18:1/FA18:2
Two-way ANOVA summary	Sex-genotype interaction	$F_{(3,24)}$=	0.1789	2.486	2.978	2.014	3.351	1.325	7.462	0.08844	5.659	1.165	1.421	0.2196	0.2084	0.8491	0.2969	1.105	1.071	2.608
		p	0.9096	0.0849	0.0515	0.1388	0.0357	0.2894	0.0011	0.9657	0.0044	0.3436	0.261	0.8818	0.8896	0.4807	0.8273	0.3666	0.3798	0.0749
	Sex factor	$F_{(1,24)}$=	2.492	0.3257	1.382	2.117	5.143	33.52	82.76	0.0049	5.798	0.4159	1.024	2.519	2.318	1.158	0.0239	1.103	2.472	23.33
		p	0.1275	0.5735	0.2512	0.1586	0.0326	<0.0001	<0.0001	0.9444	0.0241	0.5251	0.3217	0.1256	0.141	0.2927	0.3460	0.3041	0.1290	<0.0001
	Genotype factor	$F_{(3,24)}$=	125.3	260.1	63.46	69.44	27.96	21.55	49.39	82.17	71.09	59.09	28.38	70.46	71.29	74.78	127.6	45.94	20.62	20.65
		p	<0.0001	<0.0001	<0.0001	<0.0001	<0.0001	<0.0001	<0.0001	<0.0001	<0.0001	<0.0001	<0.0001	<0.0001	<0.0001	<0.0001	<0.0001	<0.0001	<0.0001	<0.0001
Post hoc Tukey's Analysis: *p*-Values for Multiple Comparisons																				
♂:$Apoe^{hA\beta}$ vs. ♂:$APOE2^{hA\beta}$			<0.0001	<0.0001	<0.0001	<0.0001	0.0031	0.5878	0.4875	<0.0001	<0.0001	<0.0001	0.0235	<0.0001	<0.0001	<0.0001	<0.0001	0.0005	0.0004	0.9965
♂:$Apoe^{hA\beta}$ vs. ♂:$APOE3^{hA\beta}$			0.2004	>0.9999	0.9901	>0.9999	0.6910	0.9265	0.5522	0.9434	>0.9999	0.7490	0.7492	0.8712	0.8751	0.9999	>0.9999	0.9996	0.5535	0.0883
♂:$Apoe^{hA\beta}$ vs. ♂:$APOE4^{hA\beta}$			>0.9999	>0.9999	0.9388	0.9998	0.9696	0.1423	0.0392	0.7406	0.9667	0.3953	0.0893	0.9918	0.9928	0.9929	0.9994	0.9889	0.7987	0.0249
♂:$Apoe^{hA\beta}$ vs. ♀:$Apoe^{hA\beta}$			0.8432	0.9904	0.4333	0.5589	0.0424	0.0050	<0.0001	>0.9999	0.0033	0.9526	0.9630	>0.9999	>0.9999	0.9966	0.9870	0.9991	>0.9999	0.0023
♂:$Apoe^{hA\beta}$ vs. ♀:$APOE2^{hA\beta}$			<0.0001	<0.0001	<0.0001	<0.0001	<0.0001	0.0007	<0.0001	<0.0001	<0.0001	0.0004	0.6346	<0.0001	<0.0001	<0.0001	<0.0001	<0.0001	0.0003	0.9993
♂:$Apoe^{hA\beta}$ vs. ♀:$APOE3^{hA\beta}$			0.0740	0.9901	0.9561	0.9989	0.9679	0.9998	>0.9999	0.7642	0.9941	0.2140	0.3535	0.1697	0.1800	0.9987	>0.9999	0.9950	0.0107	0.5901
♂:$Apoe^{hA\beta}$ vs. ♀:$APOE4^{hA\beta}$			>0.9999	0.9988	0.9991	0.9352	0.9734	0.9999	0.9656	0.7112	0.6869	0.3542	0.0285	0.8855	0.9061	0.9803	0.9996	0.9592	0.1816	0.9196
♂:$APOE2^{hA\beta}$ vs. ♂:$APOE3^{hA\beta}$			<0.0001	<0.0001	<0.0001	<0.0001	0.1396	0.0861	0.0120	<0.0001	<0.0001	<0.0001	0.0005	<0.0001	<0.0001	<0.0001	<0.0001	0.0001	0.0361	0.3085
♂:$APOE2^{hA\beta}$ vs. ♂:$APOE4^{hA\beta}$			<0.0001	<0.0001	<0.0001	<0.0001	0.0003	0.0021	0.0003	<0.0001	<0.0001	<0.0001	<0.0001	<0.0001	<0.0001	<0.0001	<0.0001	<0.0001	0.0141	0.1088
♂:$APOE2^{hA\beta}$ vs. ♀:$Apoe^{hA\beta}$			<0.0001	<0.0001	0.0002	0.0006	0.9473	0.2633	0.0002	<0.0001	0.1521	0.0002	0.2001	<0.0001	<0.0001	<0.0001	<0.0001	0.0019	0.0003	0.0004
♂:$APOE2^{hA\beta}$ vs. ♀:$APOE2^{hA\beta}$			0.9963	0.1967	0.6931	0.5118	0.6229	0.0574	0.0001	>0.9999	0.8368	0.8801	0.5854	0.9721	0.9817	0.6360	0.9638	0.5012	>0.9999	0.9158
♂:$APOE2^{hA\beta}$ vs. ♀:$APOE3^{hA\beta}$			<0.0001	<0.0001	<0.0001	<0.0001	0.0339	0.8409	0.6325	<0.0001	<0.0001	<0.0001	0.0001	<0.0001	<0.0001	<0.0001	<0.0001	<0.0001	0.8547	0.9334
♂:$APOE2^{hA\beta}$ vs. ♀:$APOE4^{hA\beta}$			<0.0001	<0.0001	<0.0001	<0.0001	0.0003	0.3461	0.0867	<0.0001	<0.0001	<0.0001	<0.0001	<0.0001	<0.0001	<0.0001	<0.0001	<0.0001	0.1672	0.9994
♂:$APOE3^{hA\beta}$ vs. ♂:$APOE4^{hA\beta}$			0.1008	>0.9999	>0.9999	>0.9999	0.1720	0.7425	0.7973	0.9997	0.9968	0.9987	0.8292	0.9991	0.9991	<0.0001	<0.0001	0.0005	0.9999	0.9988
♂:$APOE3^{hA\beta}$ vs. ♀:$Apoe^{hA\beta}$			0.9244	0.9998	0.8919	0.3764	0.6909	0.0003	<0.0001	0.8510	0.0014	0.1753	0.1923	0.9644	0.9669	0.9999	>0.9999	0.9996	0.4568	<0.0001
♂:$APOE3^{hA\beta}$ vs. ♀:$APOE2^{hA\beta}$			<0.0001	<0.0001	<0.0001	<0.0001	0.0024	<0.0001	<0.0001	<0.0001	<0.0001	<0.0001	0.0431	<0.0001	<0.0001	0.9929	0.9994	0.9889	0.0312	0.0278
♂:$APOE3^{hA\beta}$ vs. ♀:$APOE3^{hA\beta}$			0.9995	0.9998	>0.9999	>0.9999	0.9968	0.7248	0.4121	0.9998	0.9999	0.9733	0.9972	0.8679	0.8772	0.9966	0.9870	0.9991	0.4575	0.9292
♂:$APOE3^{hA\beta}$ vs. ♀:$APOE4^{hA\beta}$			0.2661	>0.9999	0.8567	0.9877	0.1797	0.9928	0.9840	0.9993	0.8652	0.9972	0.5188	>0.9999	>0.9999	<0.0001	<0.0001	<0.0001	0.9942	0.6098
♂:$APOE4^{hA\beta}$ vs. ♀:$Apoe^{hA\beta}$			0.6409	0.9998	0.9748	0.3066	0.0041	<0.0001	<0.0001	0.5802	0.0003	0.0542	0.0088	0.9997	0.9997	0.9987	>0.9999	0.9950	0.7100	<0.0001
♂:$APOE4^{hA\beta}$ vs. ♀:$APOE2^{hA\beta}$			<0.0001	<0.0001	<0.0001	<0.0001	<0.0001	<0.0001	<0.0001	<0.0001	<0.0001	<0.0001	0.0014	<0.0001	<0.0001	0.9803	0.9996	0.9592	0.0121	0.0071
♂:$APOE4^{hA\beta}$ vs. ♀:$APOE3^{hA\beta}$			0.0338	0.9998	>0.9999	>0.9999	0.4931	0.0580	0.0232	>0.9999	>0.9999	>0.9999	0.9930	0.5586	0.5678	<0.0001	<0.0001	0.0001	0.2472	0.6455
♂:$APOE4^{hA\beta}$ vs. ♀:$APOE4^{hA\beta}$			0.9993	>0.9999	0.6820	0.9957	>0.9999	0.2929	0.2865	>0.9999	0.9968	>0.9999	0.9993	0.9994	0.9997	<0.0001	<0.0001	<0.0001	0.9347	0.2804
♀:$Apoe^{hA\beta}$ vs. ♀:$APOE2^{hA\beta}$			<0.0001	<0.0001	<0.0001	<0.0001	0.1126	0.9917	>0.9999	<0.0001	0.0067	0.0058	0.9944	<0.0001	<0.0001	<0.0001	<0.0001	0.0019	0.0002	0.0084
♀:$Apoe^{hA\beta}$ vs. ♀:$APOE3^{hA\beta}$			0.6781	>0.9999	0.9629	0.2485	0.2972	0.0143	<0.0001	0.6064	0.0005	0.0229	0.0512	0.2909	0.3083	0.6360	0.9638	0.5012	0.0073	<0.0001
♀:$Apoe^{hA\beta}$ vs. ♀:$APOE4^{hA\beta}$			0.9099	>0.9999	0.1781	0.0833	0.0044	0.0018	<0.0001	0.5488	<0.0001	0.0460	0.0024	0.9704	0.9791	<0.0001	<0.0001	<0.0001	0.1351	0.0001
♀:$APOE2^{hA\beta}$ vs. ♀:$APOE3^{hA\beta}$			<0.0001	<0.0001	<0.0001	<0.0001	0.0005	0.0021	<0.0001	<0.0001	<0.0001	<0.0001	0.0094	<0.0001	<0.0001	<0.0001	<0.0001	<0.0001	0.8240	0.2880
♀:$APOE2^{hA\beta}$ vs. ♀:$APOE4^{hA\beta}$			<0.0001	<0.0001	<0.0001	<0.0001	<0.0001	0.0003	<0.0001	<0.0001	<0.0001	<0.0001	0.0004	<0.0001	<0.0001	<0.0001	<0.0001	0.0005	0.1479	0.6559
♀:$APOE3^{hA\beta}$ vs. ♀:$APOE4^{hA\beta}$			0.1039	>0.9999	0.7253	0.9988	0.5078	0.9872	0.9045	>0.9999	0.9774	>0.9999	0.8879	0.8524	0.8416	0.9999	>0.9999	0.9996	0.8803	0.9978

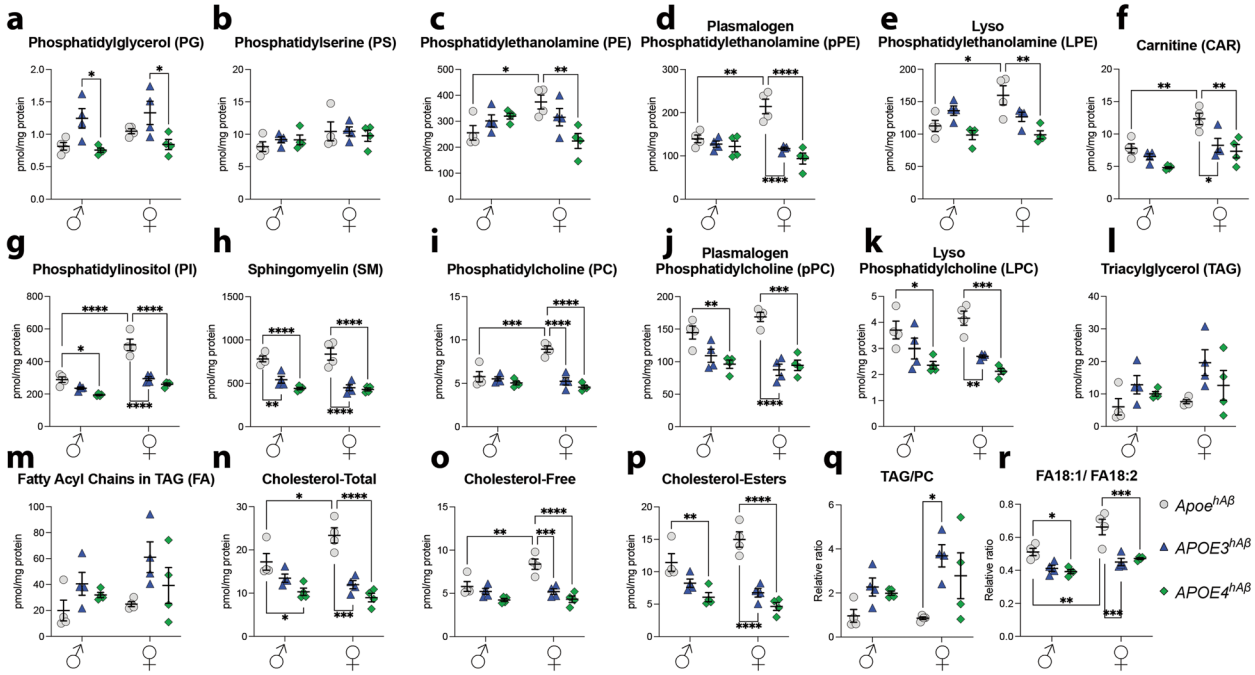

Fig. 9 Serum lipid profile of *Apoe*$^{hA\beta}$, *APOE3*$^{hA\beta}$ and *APOE4*$^{hA\beta}$ rats. Levels of PG (**a**), PS (**b**), PE (**c**), pPE (**d**), LPE (**e**), CAR (**f**), PI (**g**), SM (**h**), PC (**i**), pPC (**j**), LPC (**k**), TAG (**l**), FA (**m**), total Cholesterol (**n**), free Cholesterol (**o**) and Cholesterol esters (**p**) and relative ratios of TAG/PC (**q**) and FA18:1/FA 18:2 (**r**) in serum of 80 days old *Apoe*$^{hA\beta}$, *APOE3*$^{hA\beta}$ and *APOE4*$^{hA\beta}$ rats (n=4 per sex per genotype). Data are represented as mean ± SEM and were analyzed by two-way ANOVA followed by post hoc Tukey's multiple comparisons tests when ANOVA showed a significant difference. * $p<0.05$, ** $p<0.01$, *** $p<0.001$, **** $p<0.0001$

-0.56), there is slightly positive correlation in *APOE2*$^{hA\beta}$ rats (r= 0.018). All other correlation coefficients are reported in Additional file 2. In conclusion, our findings offer a complex picture of lipid homeostasis across *APOE* variants of rat models. The substantial variations in lipid composition could have significant implications for understanding lipid metabolism in these models, potentially serving as a basis for the identification of lipidomic biomarkers for different physiological or pathological states.

Discussion

In this study, we characterized adolescent (~80-day-old) Long-Evans rat models expressing human APOE2, APOE3, and APOE4 variants, along with humanized *App*^{h} alleles. Although LOAD manifests after the age of 65, examining these models at an early age allows us to investigate whether APOE isoforms exert early effects on critical pathways associated with LOAD. This approach aims to identify potential early biomarkers or mechanisms that could influence the risk of developing LOAD later in life.

We observed that *APOE2*$^{hA\beta}$ rats exhibited the highest levels of APOE in both serum and brain compared to *APOE4*$^{hA\beta}$ and *APOE3*$^{hA\beta}$ rats, which showed comparable levels of APOE. These changes were unlikely due to transcriptional differences, as mRNA levels of human *APOE2*, *APOE3*, and *APOE4* were comparable. Therefore, differences in protein expression are likely attributed to translational and/or protein stability variances. While further investigation into these mechanisms is warranted, these findings closely mirror observations from human studies, underscoring the validity and translatability of these rat models [58, 70, 71].

The humanization of both APP/Aβ and APOE in model organisms that express these human proteins in a physiological manner enables a comprehensive study of the multifaceted APOE-Aβ interaction. Our findings revealed a significant elevation in Aβ43 levels in male *APOE4*$^{hA\beta}$ rats compared to their *APOE2*$^{hA\beta}$ counterparts. This observation is particularly noteworthy as Aβ43 has high propensity for oligomerization and is a primary determinant of amyloid pathology [50], while APOE4 is the most prominent genetic risk factor for LOAD, increasing the risk up to 12-fold, whereas APOE2 is a protective factor [6, 72]. This finding also aligns with evidence that Aβ oligomer levels in APOE4 AD patients' brains are 2.7 times higher than those in APOE3 AD patients [73] and is consistent with findings from mouse models expressing APOE4 and APOE2 [74]. Thus, our analysis suggests that

Table 9 Statistical analysis results of Fig. 9

			PG	PS	PE	pPE	LPE	CAR	PI	SM	PC	pPC	LPC	TAG	FA	Chol. Total	Chol. Free	Chol. Esters	TAG/PC	FA18:1/FA18:2
Two-way ANOVA summary	Sex-genotype interaction	$F_{(2,18)}$=	0.3179	0.4870	8.314	12.23	5.700	1.718	12.77	1.818	15.82	3.648	1.368	0.4433	0.4383	5.507	5.915	5.055	1.102	2.596
		p	0.7317	0.6223	0.0028	0.0004	0.0121	0.2076	0.0004	0.1910	0.0001	0.0468	0.2799	0.6488	0.6519	0.0136	0.0106	0.0181	0.3537	0.1022
	Sex factor	$F_{(1,18)}$=	2.437	3.876	0.3314	1.776	2.997	20.87	64.51	0.2447	7.169	0.0014	0.0127	2.321	2.233	1.041	6.462	0.0808	2.759	19.17
		p	0.1359	0.0646	0.5719	0.1993	0.1005	0.0002	<0.0001	0.6268	0.0154	0.9701	0.9116	0.1450	0.1524	0.3212	0.0204	0.7794	0.1140	0.0004
	Genotype factor	$F_{(2,18)}$=	11.39	0.1970	1.552	21.43	10.30	13.27	52.32	52.96	26.70	32.94	22.77	5.081	5.030	34.85	22.53	39.83	8.524	22.58
		p	0.0006	0.8230	0.2388	<0.0001	0.0010	0.0003	<0.0001	<0.0001	<0.0001	<0.0001	<0.0001	0.0178	0.0184	<0.0001	<0.0001	<0.0001	0.0025	<0.0001
Post hoc Tukey's Analysis: *p*-Values for Multiple Comparisons																				
♂: $Apoe^{hA\beta}$ vs. ♂: $APOE3^{hA\beta}$			0.0904	0.9500	0.8131	0.9688	0.4556	0.8617	0.2974	0.0045	0.9969	0.0802	0.3982	0.5933	0.5935	0.3654	0.9238	0.1807	0.4950	0.1024
♂: $Apoe^{hA\beta}$ vs. ♂: $APOE4^{hA\beta}$			0.9984	0.9554	0.5305	0.8691	0.8749	0.1337	0.0120	<0.0001	0.7297	0.0089	0.0159	0.9250	0.9293	0.0165	0.1485	0.0065	0.7241	0.0359
♂: $Apoe^{hA\beta}$ vs. ♀:$Apoe^{hA\beta}$			0.6375	0.4424	0.0488	0.0019	0.0166	0.0076	<0.0001	0.9071	0.0001	0.3757	0.7907	0.9988	0.9987	0.0394	0.0052	0.1110	>0.9999	0.0052
♂: $Apoe^{hA\beta}$ vs. ♀: $APOE3^{hA\beta}$			0.0296	0.4380	0.5963	0.7043	0.8701	0.9980	0.9998	0.0001	0.9024	0.0019	0.1056	0.0424	0.0438	0.0965	0.9174	0.0196	0.0163	0.5410
♂: $Apoe^{hA\beta}$ vs. ♀: $APOE4^{hA\beta}$			>0.9999	0.7586	0.9546	0.0864	0.8854	0.9986	0.8490	<0.0001	0.2343	0.0066	0.0040	0.6192	0.6535	0.0036	0.1918	0.0006	0.1784	0.8668
♂: $APOE3^{hA\beta}$ vs. ♂: $APOE4^{hA\beta}$			0.0415	>0.9999	0.9958	0.9993	0.0763	0.6537	0.5465	0.4676	0.9330	0.8816	0.5034	0.9835	0.9819	0.5514	0.5877	0.5585	0.9987	0.9936
♂: $APOE3^{hA\beta}$ vs. ♀: $Apoe^{hA\beta}$			0.7715	0.9059	0.4048	0.0004	0.4555	0.0007	<0.0001	0.0005	<0.0001	0.0013	0.0436	0.8089	0.8133	0.0006	0.0007	0.0007	0.4115	<0.0001
♂: $APOE3^{hA\beta}$ vs. ♀: $APOE3^{hA\beta}$			0.9920	0.9031	0.9987	0.9835	0.9728	0.6362	0.1955	0.5623	0.9922	0.4890	0.9595	0.5875	0.5973	0.9623	>0.9999	0.8512	0.4121	0.8787
♂: $APOE3^{hA\beta}$ vs. ♀: $APOE4^{hA\beta}$			0.1267	0.9964	0.3384	0.3196	0.0803	0.9742	0.9085	0.3632	0.4540	0.8196	0.1972	>0.9999	>0.9999	0.2015	0.6771	0.1041	0.9795	0.5584
♂: $APOE4^{hA\beta}$ vs. ♀: $Apoe^{hA\beta}$			0.4046	0.8974	0.6925	0.0002	0.0016	<0.0001	<0.0001	<0.0001	<0.0001	0.0001	0.0011	0.9912	0.9927	<0.0001	<0.0001	<0.0001	0.6369	<0.0001
♂: $APOE4^{hA\beta}$ vs. ♀: $APOE3^{hA\beta}$			0.0129	0.8945	>0.9999	0.9994	0.2796	0.0607	0.0069	>0.9999	0.9990	0.9772	0.9263	0.2433	0.2441	0.9447	0.6002	0.9943	0.2345	0.5902
♂: $APOE4^{hA\beta}$ vs. ♀: $APOE4^{hA\beta}$			0.9909	0.9955	0.1542	0.5012	>0.9999	0.2583	0.1207	>0.9999	0.9330	>0.9999	0.9847	0.9877	0.9911	0.9764	>0.9999	0.8704	0.8802	0.2749
♀: $Apoe^{hA\beta}$ vs. ♀: $APOE3^{hA\beta}$			0.4409	>0.9999	0.6273	<0.0001	0.1459	0.0183	<0.0001	<0.0001	<0.0001	<0.0001	0.0080	0.0886	0.0929	0.0001	0.0006	<0.0001	0.0119	0.0001
♀: $Apoe^{hA\beta}$ vs. ♀: $APOE4^{hA\beta}$			0.7442	0.9936	0.0086	<0.0001	0.0017	0.0033	<0.0001	<0.0001	<0.0001	0.0001	0.0003	0.8299	0.8595	<0.0001	<0.0001	<0.0001	0.1378	0.0005
♀: $APOE3^{hA\beta}$ vs. ♀: $APOE4^{hA\beta}$			0.0429	0.9931	0.1862	0.6945	0.2910	0.9609	0.7114	0.9991	0.7823	0.9914	0.6031	0.5616	0.5374	0.6024	0.6893	0.5854	0.8127	0.9902

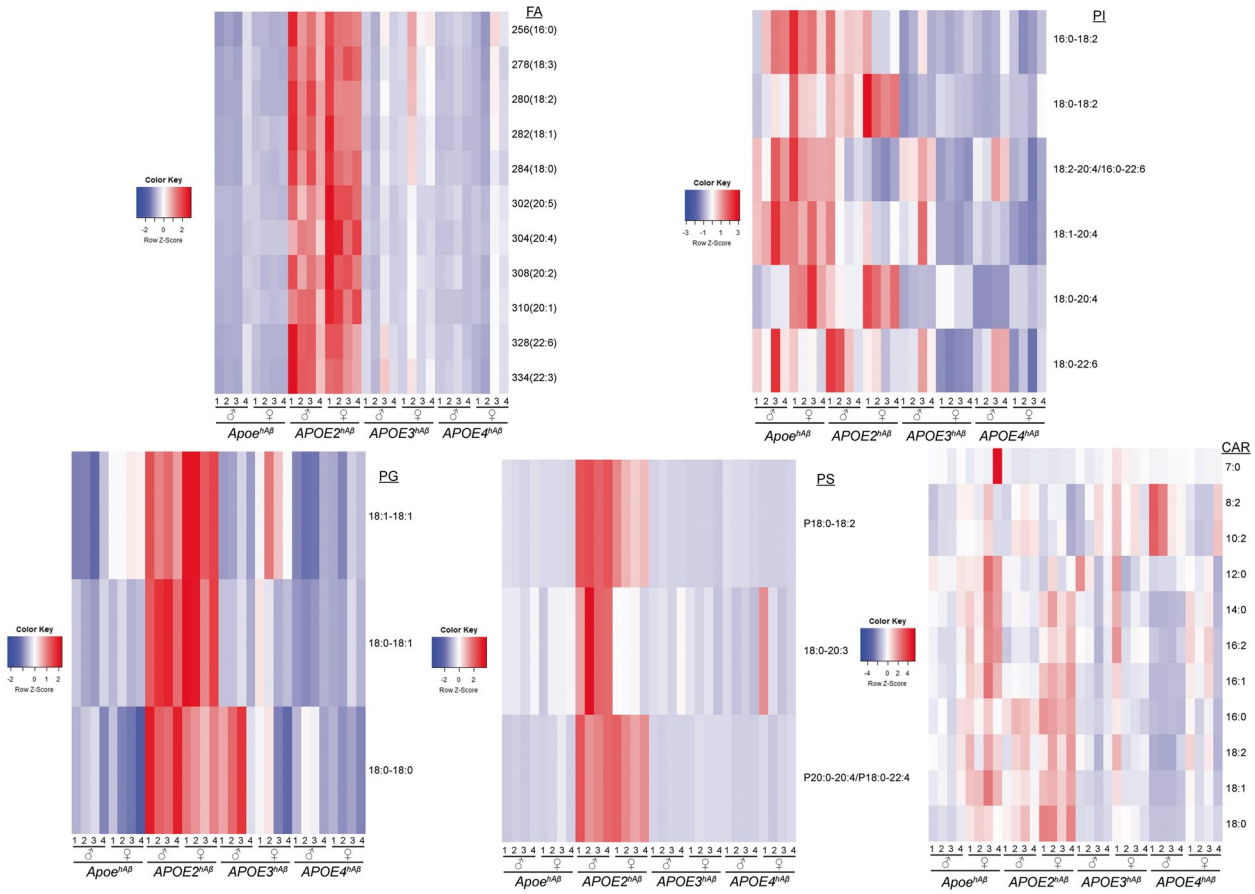

Fig. 10 Heatmap analysis of FA, PI, PG, PS, and CAR in serum of individual rats. Heatmap represents the relative levels of various lipids. Each row corresponds to a specific lipid, and each column corresponds to an individual rat. The color of each cell indicates the relative change from the mean of the same row (lipid) across all individuals. The color gradient ranges from dark blue (lowest) to red (highest). Blue colors represent lower relative levels of a particular lipid in an individual, while red colors indicate higher relative levels

APP processing and metabolism may be influenced by APOE isoforms early in life, potentially revealing alterations that precede the onset of LOAD by decades.

Tau is believed to play a key role in *APOE4*-related neuronal alterations during aging, as *APOE4* leads to age- and Tau-dependent impairment of hilar GABAergic interneurons, resulting in learning and memory deficits in mice [75]. We observed a decrease in Tau levels in APOE variant-carrying males compared to $Apoe^{hA\beta}$ males, with Tau also being lower in $APOE4^{hA\beta}$ females compared to $Apoe^{hA\beta}$ females. Additionally, phosphorylated Tau at $pS^{396\text{-}404}$ was decreased in $APOE4^{hA\beta}$ males compared to $Apoe^{hA\beta}$ males. However, we did not observe significant human APOE isoform-dependent changes in total Tau or in phosphorylated Tau species. This suggests that APOE4 impact on Tau pathology may not become measurable until later in life.

Neuroinflammation is another feature of AD pathology. Numerous cytokines and chemokines are expressed at abnormal levels in AD [76]. In APOE4 carriers, chronic inflammation has been linked to an accelerated onset of AD symptoms [77]. In our study, we observed modest variations in cytokine levels across APOE isoforms and sexes. Specifically, male $APOE2^{hA\beta}$ rats exhibited slightly reduced levels of anti-inflammatory cytokines such as IL13, IL4 and IL4, compared to $APOE4^{hA\beta}$ rats. Also, male $APOE2^{hA\beta}$ rats showed lower levels of IFNγ, IL6, and Cxcl1 compared to their female counterparts. Previous studies utilizing intracerebroventricular LPS injections have demonstrated significant increases in pro-inflammatory cytokines (IL1β, IL6, TNFα), particularly in *APOE4* mice [78]. However, in adolescent models, the expected increase in neuroinflammation associated with APOE4 was not observed, suggesting that APOE4's impact on neuroinflammation may not become obvious until later in life and/or may require specific inflammatory triggers.

Previous studies have reported LTP deficits in *APOE4*-carrying mice compared to *APOE3*-carrying mice, in addition to morphological alterations in CA1

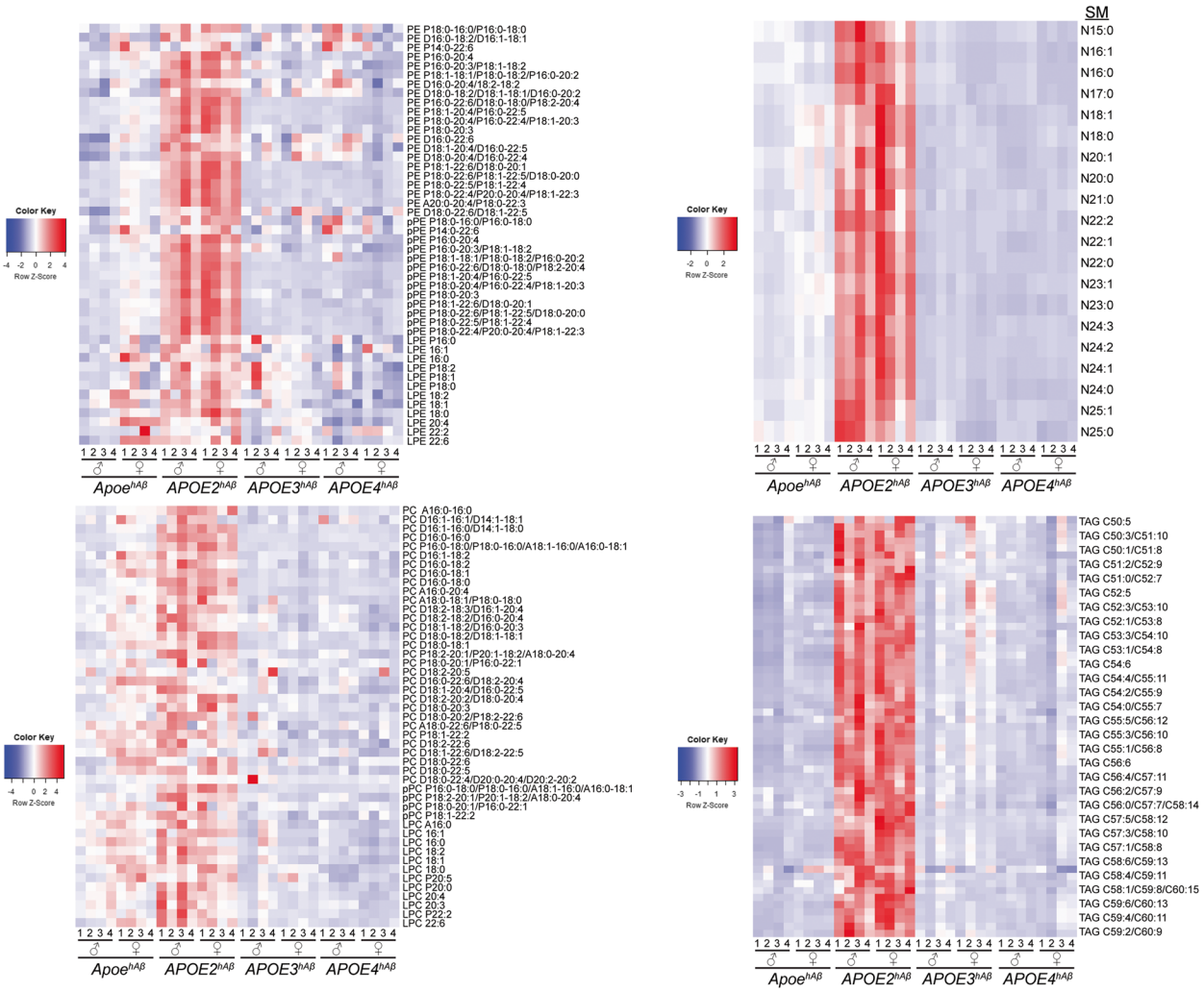

Fig. 11 Heatmap analysis of PE and related lipid species, SM, PC and related lipid species, and TAG in serum of individual rats. Heatmap represents the relative levels of various lipids. Each row corresponds to a specific lipid, and each column corresponds to an individual rat. The color of each cell indicates the relative change from the mean of the same row (lipid) across all individuals. The color gradient ranges from dark blue (lowest) to red (highest). Blue colors represent lower relative levels of a particular lipid in an individual, while red colors indicate higher relative levels

hippocampal neurons such as shortened dendritic length, reduced spine density, decreased levels of the presynaptic glutamatergic transporter vGLUT and GABAergic interneuron loss [79–81]. *APOE4*$^{hA\beta}$ rats also exhibited increased neuronal excitability compared to *Apoe*$^{hA\beta}$ rats and LTP deficit relative to both *APOE3*$^{hA\beta}$ and *Apoe*$^{hA\beta}$ rats, aligning our findings with previous studies. *APOE2*$^{hA\beta}$ rats exhibited similar deficits in LTP as *APOE4*$^{hA\beta}$ rats. This finding is consistent with observations reported in APOE2-carrying mice [82], but appears paradoxical given APOE2's typical association with neuroprotection in AD [83, 84]. The observed dysregulation in lipid metabolism in *APOE2*$^{hA\beta}$ rats may account for this result, as altered brain lipidomics in these rats could significantly impact synaptic transmission. The potential protective function of APOE2 might be more effectively studied in rats heterozygous for APOE2 and APOE4, as this could mitigate or eliminate the pronounced lipidomic alterations associated with APOE2. Future studies are needed to explore this hypothesis further. Despite these findings, the early LTP deficits observed in *APOE4*$^{hA\beta}$ rats could signify an initial stage of a pathological process that may precede the development of full-blown AD pathology.

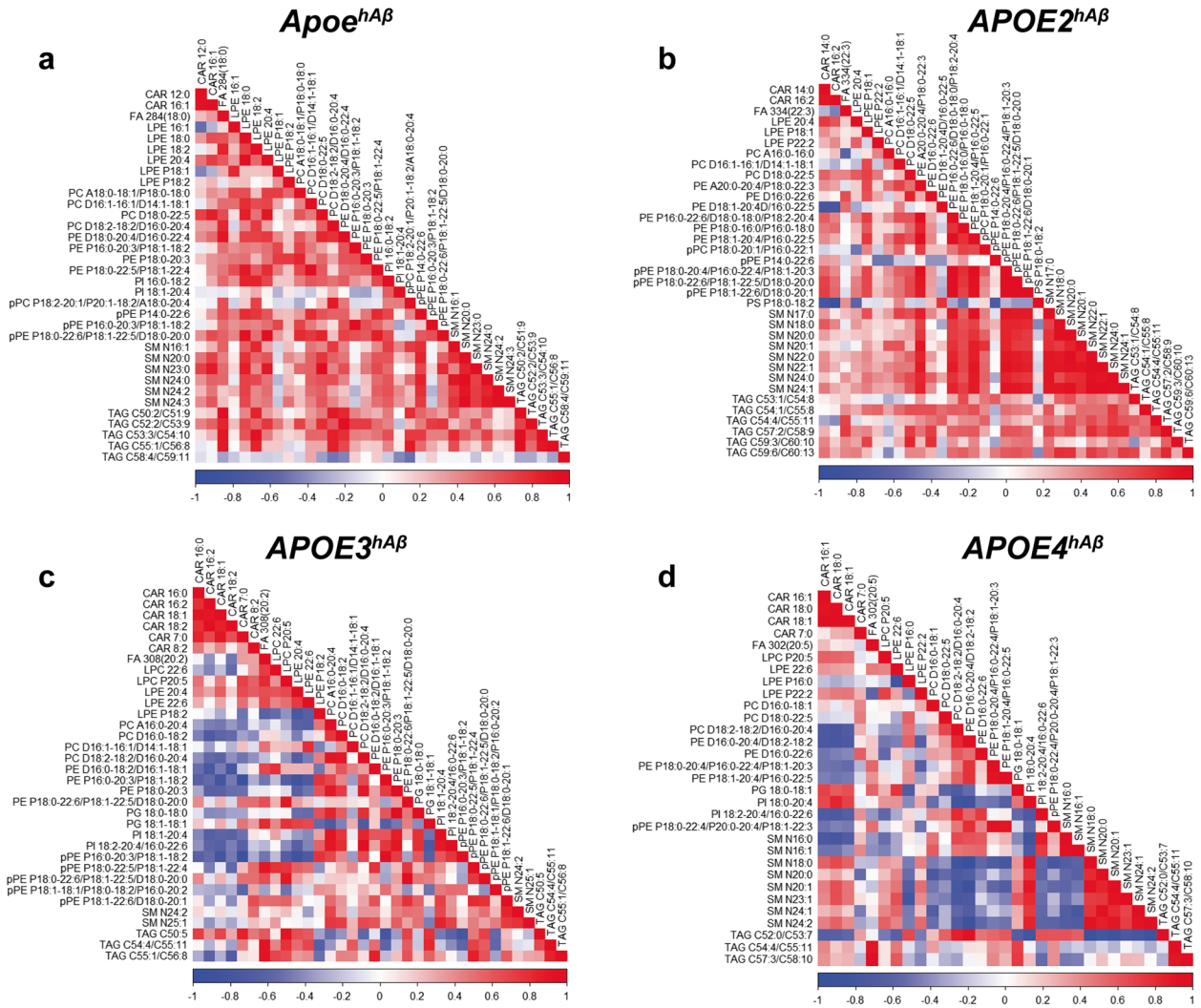

Fig. 12 Correlation heatmaps of top 20 correlations with $p<0.05$ for *Apoe*^{hAβ}, *APOE2*^{hAβ}, *APOE3*^{hAβ} and *APOE4*^{hAβ} rats. All correlation coefficients are reported in Additional file 2

APOE2 homozygosity can lead to type III HLP in humans. Our findings suggest that *APOE2*^{hAβ} rats serve as a suitable model for studying this condition, showing elevated triglyceride and cholesterol levels. This led us to investigate how different human *APOE* isoforms affect lipid metabolism in models expressing humanized APOE variants and humanized APP/Aβ in a more comprehensive manner. Our findings confirm the elevated lipid levels previously observed in humanized *APOE2* mice compared to those carrying *APOE3* and *APOE4* [85]. Moreover, we identified significant differences with the mouse models, including notably higher serum levels of total PG, pPE, LPE, CAR, PI, PC, pPC, LPC, FA in TAG, free-cholesterol, and cholesterol-esters. These observations are consistent with data showing that brain samples from *APOE2* LOAD patients exhibit elevated levels of CAR, SM, PC, and LPE compared to *APOE3* and *APOE4* LOAD patients [86]. Thus, rats, known for their more human-like metabolism compared to mice [54], and engineered to carry human *APOE2* along with the humanized *App* gene, may offer enhanced modeling capabilities for type III HLP compared to their mouse counterparts.

A follow-up analysis aimed at discerning differences between *APOE3*^{hAβ} and *APOE4*^{hAβ} rats revealed that only PG levels were lower in both male and female *APOE3*^{hAβ} rats compared to *APOE4*^{hAβ} animals. All other lipid categories showed no significant variation between these two groups. This serum lipidomic similarity between *APOE4*^{hAβ} and *APOE3*^{hAβ} rats mirrors the lipid homogeneity observed in synaptosomes

isolated from 2-month-old mice expressing human *APOE3* and *APOE4* [87].

One limitation of this study is that, although significant deficits in STP and early LTP were observed, late LTP did not reach statistical significance in $APOE4^{hA}$ rats, possibly due to experimental variability. Additionally, while we detected lipidomic changes in the serum, we did not investigate whether these alterations are mirrored in the brain. Future studies should include a comparative lipidomic analysis of both serum and brain tissue to clarify the extent of these changes in the central nervous system. Furthermore, we did not examine how the elevated lipid levels in $APOE2^{hA\beta}$ rats may affect other systems/organs, including the potential for atherosclerosis development. Exploring these systemic effects will enhance our understanding of the broader impact of lipid changes beyond the brain. Finally a longitudinal analysis extending to behavioral studies that assess learning and memory will be essential for a more comprehensive characterization of these models.

Conclusions

In this study, we utilized Long-Evans knock-in rats with humanized *App* and *APOE2*, *APOE3*, and *APOE4* isoforms to investigate their early roles in LOAD and type III HLP. Our findings reveal distinct profiles of APOE expression and lipid metabolism associated with each *APOE* isoform. Specifically, $APOE2^{hA\beta}$ rats exhibited higher APOE levels in both serum and brain compared to $APOE4^{hA\beta}$ and $APOE3^{hA\beta}$ rats, suggesting isoform-specific differences in protein expression likely due to translational or stability factors rather than transcriptional differences.

Notably, elevated Aβ43 levels were observed in male $APOE4^{hA\beta}$ rats, which could precede amyloid pathology due to Aβ43's high aggregation propensity. Additionally, the early LTP deficits observed in $APOE4^{hA\beta}$ rats may represent an early-stage pathogenic mechanism that could evolve into LOAD. Furthermore, $APOE2^{hA\beta}$ rats showed elevated triglyceride and cholesterol levels, supporting their utility as a model for type III HLP. Minimal lipid profile differences between $APOE4^{hA\beta}$ and $APOE3^{hA\beta}$ rats reflect previously observed patterns in mouse models

Overall, these rat models provide a valuable platform for exploring the interactions between human *APOE* isoforms and Aβ in the context of LOAD and lipid metabolism. Future studies will expand lipidomic analyses to various CNS regions, offering deeper insights into the effects of human APOE isoforms on lipid metabolism and Alzheimer's disease pathology. Comparing the brain lipidomic of $APOE2^{hA\beta}$, $APOE3^{hA\beta}$ and $APOE4^{hA\beta}$ rats with lipidomic profiles from postmortem AD brains will further validate the translatability of the models described here [86].

Supplementary Information

The online version contains supplementary material available at https://doi.org/10.1186/s12964-024-01832-2.

Additional file 1.

Additional file 2.

Additional file 3.

Authors' contributions

MY and LD wrote the first draft of the manuscript. MY, TY, MT, HB, MP, and LD contributed to the material preparation, data collection, and figure drawing. MY, TY, MT, XH, and LD contributed to the critical review of the manuscript. LG and CD contributed material and expertise for Tau analysis. All authors reviewed and approved the final version.

Funding

MY: Alzheimer's Association, 24AARFD-1243865
XH: National Institute on Aging, R01AG061729; National Institutes of Health, P30 AG013319
LD: National Institute on Aging, R01AG073182; National Institute on Aging, R01AG063407; National Institute on Aging, RF1AG064821

Availability of data and materials

No datasets were generated or analysed during the current study.

Declarations

Competing interests

The authors declare no competing interests.

Author details

[1]Department of Pharmacology, Physiology & Neuroscience New Jersey Medical School, The State University of New Jersey, Rutgers, Newark, NJ, USA. [2]Barshop Institute for Longevity and Aging Studies, University of Texas Health San Antonio, San Antonio, TX 78229, USA. [3]Litwin-Zucker Center for the Study of Alzheimer's Disease and Memory Disorders, Feinstein Institutes for Medical Research, Institute of Molecular Medicine, Manhasset, NY, USA. [4]Institute of Neurology and Neurosurgery, Northwell Health System, Manhasset, NY, USA. [5]Department of Medicine - Diabetes, University of Texas Health San Antonio, San Antonio, TX 78229, USA.

Received: 23 July 2024 Accepted: 15 September 2024
Published online: 27 September 2024

References

1. Yamazaki Y, et al. Apolipoprotein E and Alzheimer disease: pathobiology and targeting strategies. Nat Rev Neurol. 2019;15(9):501–18.
2. Huebbe P, Rimbach G. Evolution of human apolipoprotein E (APOE) isoforms: gene structure, protein function and interaction with dietary factors. Ageing Res Rev. 2017;37:146–61.
3. Fullerton SM, et al. Apolipoprotein E variation at the sequence haplotype level: implications for the origin and maintenance of a major human polymorphism. Am J Hum Genet. 2000;67(4):881–900.
4. Kayden HJ, Maschio F, Traber MG. The secretion of apolipoprotein E by human monocytederived macrophages. Arch Biochem Biophys. 1985;239(2):388–95.
5. Gee JR, Keller JN. Astrocytes: regulation of brain homeostasis via apolipoprotein E. Int J Biochem Cell Biol. 2005;37(6):1145–50.
6. West HL, Rebeck GW, Hyman BT. Frequency of the apolipoprotein E ε2 allele is diminished in sporadic Alzheimer disease. Neurosci Lett. 1994;175(1–2):46–8.
7. Farrer LA, et al. Effects of age, sex, and ethnicity on the association between apolipoprotein E genotype and Alzheimer disease: a meta-analysis. JAMA. 1997;278(16):1349–56.
8. Kojro E, et al. Low cholesterol stimulates the nonamyloidogenic pathway by its effect on the α-secretase ADAM 10. Proc Natl Acad Sci. 2001;98(10):5815–20.

9. Grösgen S, et al. Role of amyloid beta in lipid homeostasis. Biochim Biophys Acta Mol Cell Biol Lipids. 2010;1801(8):966–74.
10. Cordy JM, et al. Exclusively targeting β-secretase to lipid rafts by GPI-anchor addition up-regulates β-site processing of the amyloid precursor protein. Proc Natl Acad Sci. 2003;100(20):11735–40.
11. LaDu MJ, et al. Isoform-specific binding of apolipoprotein E to beta-amyloid. J Biol Chem. 1994;269(38):23403–6.
12. Sharman MJ, et al. APOE genotype results in differential effects on the peripheral clearance of amyloid-β 42 in APOE knock-in and knock-out mice. J Alzheimers Dis. 2010;21(2):403–9.
13. Tambini MD, Yao W, D'Adamio L. Facilitation of glutamate, but not GABA, release in familial Alzheimer's APP mutant Knock-in rats with increased beta-cleavage of APP. Aging Cell. 2019;18(6):e13033.
14. Piedrahita JA, et al. Generation of mice carrying a mutant apolipoprotein E gene inactivated by gene targeting in embryonic stem cells. Proc Natl Acad Sci. 1992;89(10):4471–5.
15. Sullivan PM, et al. Targeted replacement of the mouse apolipoprotein E gene with the common human APOE3 allele enhances diet-induced hypercholesterolemia and atherosclerosis. J Biol Chem. 1997;272(29):17972–80.
16. Wu Y, et al. Features of lipid metabolism in humanized ApoE knockin rat models. Int J Mol Sci. 2021;22(15):8262.
17. Deacon RM. Housing, husbandry and handling of rodents for behavioral experiments. Nat Protoc. 2006;1(2):936–46.
18. Whishaw IQ, et al. Accelerated nervous system development contributes to behavioral efficiency in the laboratory mouse: a behavioral review and theoretical proposal. Dev Psychobiol. 2001;39(3):151–70.
19. Kepecs A, et al. Neural correlates, computation and behavioural impact of decision confidence. Nature. 2008;455(7210):227–31.
20. Jemstedt A, Schwartz BL, Jonsson FU. Ease-of-learning judgments are based on both processing fluency and beliefs. Memory. 2018;26(6):807–15.
21. Bartelle BB, Barandov A, Jasanoff A. Molecular fMRI. J Neurosci. 2016;36(15):4139–48.
22. Zimmer ER, et al. In vivo tracking of tau pathology using positron emission tomography (PET) molecular imaging in small animals. Transl Neurodegener. 2014;3(1):6.
23. Leuzy A, et al. Use of amyloid PET across the spectrum of Alzheimer's disease: clinical utility and associated ethical issues. Amyloid. 2014;21(3):143–8.
24. Zimmer ER, et al. Developments in Tau PET imaging. Can J Neurol Sci. 2014;41(5):547–53.
25. Andreadis A. Tau gene alternative splicing: expression patterns, regulation and modulation of function in normal brain and neurodegenerative diseases. Biochim Biophys Acta. 2005;1739(2–3):91–103.
26. Janke C, et al. Phylogenetic diversity of the expression of the microtubule-associated protein tau: implications for neurodegenerative disorders. Brain Res Mol Brain Res. 1999;68(1–2):119–28.
27. Hong M, et al. Mutation-specific functional impairments in distinct tau isoforms of hereditary FTDP-17. Science. 1998;282(5395):1914–7.
28. Hanes J, et al. Rat tau proteome consists of six tau isoforms: implication for animal models of human tauopathies. J Neurochem. 2009;108(5):1167–76.
29. McMillan P, et al. Tau isoform regulation is region- and cell-specific in mouse brain. J Comp Neurol. 2008;511(6):788–803.
30. Mahley RW, Huang Y, Rall SC. Pathogenesis of type III hyperlipoproteinemia (dysbetalipoproteinemia): questions, quandaries, and paradoxes. J Lipid Res. 1999;40(11):1933–49.
31. Mahley RW, Ji Z-S. Remnant lipoprotein metabolism: key pathways involving cell-surface heparan sulfate proteoglycans and apolipoprotein E. J Lipid Res. 1999;40(1):1–16.
32. Lund-Katz S, et al. Apolipoprotein B-100 conformation and particle surface charge in human LDL subspecies: implication for LDL receptor interaction. Biochemistry. 1998;37(37):12867–74.
33. Huang Y, et al. Overexpression and accumulation of apolipoprotein E as a cause of hypertriglyceridemia *. J Biol Chem. 1998;273(41):26388–93.
34. Rensen PCN, van Berkel TJC. Apolipoprotein E effectively inhibits lipoprotein lipase-mediated lipolysis of chylomicron-like triglyceride-rich lipid emulsions in vitro and in vivo. J Biol Chem. 1996;271(25):14791–9.
35. Fredrickson DS, Levy RI, Lees RS. Fat transport in lipoproteins — an integrated approach to mechanisms and disorders. N Engl J Med. 1967;276(3):148–56.
36. Utermann G, Jaeschke M, Menzel J. Familial hyperlipoproteinemia type III: deficiency of a specific apolipoprotein (apo E-III) in the very-low-density lipoproteins. FEBS lett. 1975;56(2):352–5.
37. Zannis VI, Breslow JL. Human very low density lipoprotein apolipoprotein E isoprotein polymorphism is explained by genetic variation and post-translational modification. Biochemistry. 1981;20(4):1033–41.
38. Mahley RW. Apolipoprotein E: cholesterol transport protein with expanding role in cell biology. Science. 1988;240(4852):622–30.
39. Davignon J, Gregg RE, Sing CF. Apolipoprotein E polymorphism and atherosclerosis. Arteriosclerosis. 1988;8(1):1–21.
40. Phillips MC. Apolipoprotein E isoforms and lipoprotein metabolism. IUBMB Life. 2014;66(9):616–23.
41. Gustavsson J, et al. Interaction of apolipoprotein E genotype with smoking and physical inactivity on coronary heart disease risk in men and women. Atherosclerosis. 2012;220(2):486–92.
42. Weisgraber KH, Innerarity TL, Mahley RW. Abnormal lipoprotein receptor-binding activity of the human E apoprotein due to cysteine-arginine interchange at a single site. J Biol Chem. 1982;257(5):2518–21.
43. Pham H, Yin T, D'Adamio L. Initial assessment of the spatial learning, reversal, and sequencing task capabilities of knock-in rats with humanizing mutations in the Aβ-coding region of App. PLoS One. 2022;17(5):e0263546.
44. Tambini MD, Yao W, D'Adamio L. Facilitation of glutamate, but not GABA, release in familial Alzheimer's APP mutant knock-in rats with increased β-cleavage of APP. Aging Cell. 2019;18(6):e13033.
45. Yesiltepe M, et al. Late-long-term potentiation magnitude, but not Abeta levels and amyloid pathology, is associated with behavioral performance in a rat knock-in model of Alzheimer disease. Front Aging Neurosci. 2022;14:1040576.
46. Tambini MD, et al. Abeta43 levels determine the onset of pathological amyloid deposition. J Biol Chem. 2023;299(7):104868.
47. Yin T, et al. A familial Danish dementia rat shows impaired presynaptic and postsynaptic glutamatergic transmission. J Biol Chem. 2021;297(3):101089.
48. Ren S, et al. TNF-alpha-mediated reduction in inhibitory neurotransmission precedes sporadic Alzheimer's disease pathology in young Trem 2(R47H) rats. J Biol Chem. 2021;296:100089.
49. Ren S, et al. Microglia TREM2(R47H) Alzheimer-linked variant enhances excitatory transmission and reduces LTP via increased TNF-alpha levels. Elife. 2020;9:e57513.
50. Tambini MD, et al. Aβ43 levels determine the onset of pathological amyloid deposition. J Biol Chem. 2023;299(7):104868.
51. Yesiltepe M, et al. Late-long-term potentiation magnitude, but not Aβ levels and amyloid pathology, is associated with behavioral performance in a rat knock-in model of Alzheimer disease. Front Aging Neurosci. 2022;14:1040576.
52. Han X. Lipidomics: comprehensive mass spectrometry of lipids. Hoboken: Wiley; 2016.
53. Palavicini JP, et al. Novel molecular insights into the critical role of sulfatide in myelin maintenance/function. J Neurochem. 2016;139(1):40–54.
54. Han X, Yang K, Gross RW. Microfluidics-based electrospray ionization enhances the intrasource separation of lipid classes and extends identification of individual molecular species through multi-dimensional mass spectrometry: development of an automated high-throughput platform for shotgun lipidomics. Rapid Commun Mass Spectrom. 2008;22(13):2115–24.
55. Yang K, et al. Automated lipid identification and quantification by multidimensional mass spectrometry-based shotgun lipidomics. Anal Chem. 2009;81(11):4356–68.
56. Wang M, Han X. Multidimensional mass spectrometry-based shotgun lipidomics. Methods Mol Biol. 2014;1198:203–20.
57. Yang K, et al. Automated lipid identification and quantification by multidimensional mass spectrometry-based shotgun lipidomics. Anal Chem. 2009;81(11):4356–68.
58. Cai C, Wen Z, Li L. The relationship between ApoE gene polymorphism and the efficacy of statins controlling hyperlipidemia. Am J Transl Res. 2021;13(6):6772–7.
59. Passer B, et al. Generation of an apoptotic intracellular peptide by gamma-secretase cleavage of Alzheimer's amyloid beta protein precursor. J Alzheimers Dis. 2000;2(3–4):289–301.

60. Cleveland DW, Hwo S-Y, Kirschner MW. Physical and chemical properties of purified tau factor and the role of tau in microtubule assembly. J Mol Biol. 1977;116(2):227–47.
61. Noble W, et al. The importance of tau phosphorylation for neurodegenerative diseases. Front Neurol. 2013;4:83.
62. Biundo F, et al. A role for tau in learning, memory and synaptic plasticity. Sci Rep. 2018;8(1):3184.
63. Grundke-Iqbal I, et al. Abnormal phosphorylation of the microtubule-associated protein tau (tau) in Alzheimer cytoskeletal pathology. Proc Natl Acad Sci. 1986;83(13):4913–7.
64. Tzioras M, et al. Invited review: APOE at the interface of inflammation, neurodegeneration and pathological protein spread in Alzheimer's disease. Neuropathol Appl Neurobiol. 2019;45(4):327–46.
65. Keene CD, et al. Apolipoprotein E isoforms and regulation of the innate immune response in brain of patients with Alzheimer's disease. Curr Opin Neurobiol. 2011;21(6):920–8.
66. Gorelick PB. Role of inflammation in cognitive impairment: results of observational epidemiological studies and clinical trials. Ann N Y Acad Sci. 2010;1207:155–62.
67. Tai LM, et al. modulated Aβ-induced neuroinflammation in Alzheimer's disease: current landscape, novel data, and future perspective. J Neurochem. 2015;133(4):465–88.
68. Krzywkowski P, et al. Cholinergic systems and long-term potentiation in memory-impaired apolipoprotein E-deficient mice. Neuroscience. 1999;92(4):1273–86.
69. Kinosian B, Glick H, Garland G. Cholesterol and coronary heart disease: predicting risks by levels and ratios. Ann Intern Med. 1994;121(9):641–7.
70. Martínez-Morillo E, et al. Total apolipoprotein E levels and specific isoform composition in cerebrospinal fluid and plasma from Alzheimer's disease patients and controls. Acta Neuropathol. 2014;127(5):633–43.
71. Giannisis A, et al. Plasma apolipoprotein E levels, isoform composition, and dimer profile in relation to plasma lipids in racially diverse patients with Alzheimer's disease and mild cognitive impairment. Alzheimers Res Ther. 2023;15(1):119.
72. Michaelson DM. APOE ε4: the most prevalent yet understudied risk factor for Alzheimer's disease. Alzheimers Dement. 2014;10(6):861–8.
73. Hashimoto T, et al. Apolipoprotein E, especially apolipoprotein E4, increases the oligomerization of amyloid β peptide. J Neurosci. 2012;32(43):15181–92.
74. Hudry E, et al. Gene transfer of human Apoe isoforms results in differential modulation of amyloid deposition and neurotoxicity in mouse brain. Sci Transl Med. 2013;5(212):212ra161-212ra161.
75. Andrews-Zwilling Y, et al. Apolipoprotein E4 causes age- and Tau-dependent impairment of GABAergic interneurons, leading to learning and memory deficits in mice. J Neurosci. 2010;30(41):13707.
76. Wyss-Coray T, Rogers J. Inflammation in Alzheimer disease—a brief review of the basic science and clinical literature. Cold Spring Harb Perspect Med 2012;2(1):a006346.
77. Tao Q, et al. Association of chronic low-grade inflammation with risk of Alzheimer disease in ApoE4 carriers. JAMA Netw Open. 2018;1(6):e183597–e183597.
78. Zhu Y, et al. APOE genotype alters glial activation and loss of synaptic markers in mice. Glia. 2012;60(4):559–69.
79. Sun G-Z, et al. Hippocampal synaptic and neural network deficits in young mice carrying the human 4 gene. CNS Neurosci Ther. 2017;23(9):748–58.
80. Liraz O, Boehm-Cagan A, Michaelson DM. ApoE4 induces Aβ42, tau, and neuronal pathology in the hippocampus of young targeted replacement apoE4 mice. Mol Neurodegener. 2013;8(1):16.
81. Najm R, Jones EA, Huang Y. Apolipoprotein E4, inhibitory network dysfunction, and Alzheimer's disease. Mol Neurodegener. 2019;14(1):24.
82. Trommer BL, et al. ApoE isoform affects LTP in human targeted replacement mice. Neuroreport. 2004;15(17):2655–8.
83. Conejero-Goldberg C, et al. APOE2 enhances neuroprotection against Alzheimer's disease through multiple molecular mechanisms. Mol Psychiatry. 2014;19(11):1243–50.
84. Trommer BL, et al. ApoE isoform-specific effects on LTP: blockade by oligomeric amyloid-beta1-42. Neurobiol Dis. 2005;18(1):75–82.
85. Sharman MJ, et al. Profiling brain and plasma lipids in human apoe ε2, ε3, and ε4 knock-in mice using electrospray ionization mass spectrometry. J Alzheimers Dis. 2010;20(1):105–11.
86. Lefterov I, et al. APOE2 orchestrated differences in transcriptomic and lipidomic profiles of postmortem AD brain. Alzheimers Res Ther. 2019;11(1):113.
87. Igbavboa U, et al. Murine synaptosomal lipid raft protein and lipid composition are altered by expression of human apoE 3 and 4 and by increasing age. J Neurol Sci. 2005;229:225–32.

Publisher's Note